REPORT DOCUMENTATION PAGE

Form Approved
OMB No. 074-0188

1. AGENCY USE ONLY (Leave blank)	2. REPORT DATE	3. REPORT TYPE AND DATES COVERED
	November 30, 2011	Final Report; 5/1/08 – 11/30/11

4. TITLE AND SUBTITLE
Basic Research on Plasma Cathode for HPM Sources (NE- Luginsland)

5. FUNDING NUMBERS
FA9550-08-1-0045

6. AUTHOR(S)
Robert A. Schill, Jr. (PI)

7. PERFORMING ORGANIZATION NAME(S) AND ADDRESS(ES)
University of Nevada Las Vegas
Electrical and Computer Engineering
4505 Maryland Parkway
Las Vegas, Nevada 89154-4026

8. PERFORMING ORGANIZATION REPORT NUMBER
DNA

9. SPONSORING / MONITORING AGENCY NAME(S) AND ADDRESS(ES)
AFOSR/NE
875 N. Randolph St, Rm 3-112
Arlington, VA 22203

10. SPONSORING / MONITORING AGENCY REPORT NUMBER
AFRL-OSR-VA-TR-2012-0207

11. SUPPLEMENTARY NOTES

12a. DISTRIBUTION / AVAILABILITY STATEMENT
A

12b. DISTRIBUTION CODE
DIST CODE A: UNLIMITED

13. ABSTRACT ***(Maximum 200 Words)***

This grant aided in the design, construction, and operation of the UNLV Non-Equilibrium Plasma Pinch (NEPP) to be used for the study of basic research on plasma cathodes. Significantly strong pinches have been recorded. A UNLV patent pending beam management device was conceived, developed, and built to focus high energy, large electron population beams without the aid of an external magnetic field. Further, a technique was theoretically and experimentally developed to calibrate the UNLV patented EM dots used to measure time varying electric and magnetic field signatures simultaneously at one point in space in support of pinch experiments. A multiple space/time-scale technique based on a multiple fluid approach has been developed to study non-equilibrium plasma pinch physics. Non-equilibrium zero order expressions have been established laying the foundation for higher order effects based on the existence of a sheet current plasma sheath. Three high school teacher summer research experiences were funded in support of basic plasma cathode research. Their equilibrium plasma discharge studies suggest a pinch mechanism responsible for the stable pinches observed in their experiments. This has lead to theoretical and experimental equilibrium pinch studies performed in parallel with the non-equilibrium studies. Verification studies are underway. Results are reported.

14. SUBJECT TERMS	15. NUMBER OF PAGES
	36
	16. PRICE CODE

17. SECURITY CLASSIFICATION OF REPORT	18. SECURITY CLASSIFICATION OF THIS PAGE	19. SECURITY CLASSIFICATION OF ABSTRACT	20. LIMITATION OF ABSTRACT

Annual Report Period 5/1/09 – 4/30/10

Grant No.: FA9550-08-1-0045

Basic Research on Plasma Cathode for HPM Sources (NE- Luginsland)

by

Robert A. Schill, Jr., Professor
Director of Energy Materials Interaction Technology
Initiative of Nevada (EMITION) Center
University of Nevada Las Vegas
Department of Electrical and Computer Engineering
4505 Maryland Parkway
Las Vegas, Nevada 89154-4026
Phone: (702) 895-1526
FAX: (702) 895-4075
E-mail: schill@ee.unlv.edu
Lab URL: http://EMandPPLabs.nscee.edu

Abstract

This grant aided in the design, construction, and operation of the UNLV Non-Equilibrium Plasma Pinch (NEPP) to be used for the study of basic research on plasma cathodes for high power microwave sources. Significantly strong pinches have been recorded experimentally. A UNLV patent pending beam management device was conceived, developed, and built to focus high energy, large electron population beams without the aid of an external magnetic field. Further, a technique was theoretically and experimentally developed to calibrate the UNLV patented EM dots used to measure time varying electric and magnetic field signatures simultaneously at one point in space in support of pinch experiments. A multiple space/time-scale technique based on a multiple fluid approach has been developed to study non-equilibrium plasma pinch physics. Non-equilibrium zero order expressions have been established laying the foundation for higher order effects based on the existence of a sheet current plasma sheath. Three high school teacher summer research experiences were funded in support of basic plasma cathode research. Their equilibrium plasma discharge studies suggest a pinch mechanism responsible for the stable pinches observed in their experiments. This has lead to theoretical and experimental equilibrium pinch studies performed in parallel with the non-equilibrium studies. Verification studies are underway. Results are reported.

I. Introduction

Grant number FA9550-08-1-0045 provides funding to investigate basic research on a plasma cathode with applications to slow wave structure (SWS) and cross-field high power microwave tube devices such as, for example, the PASOTRON and magnetron. The plasma cathode responsible for electron production is generated in a dense Non-Equilibrium Plasma Pinch (NEPP). Embodied in the form of questions, the following two hypotheses encompass the spirit and goal of the funded research effort:

- *Does a controllable, basic interaction coupling mechanism exist in a non-equilibrium plasma pinch that can be exploited for electron production and extraction with beam management to drive high power microwave devices (typically high vacuum and/or low vacuum slow wave devices and cross field devices) in burst mode? Here, burst mode effectively implies an impulse-like (short pulse duration), intense, highly populated electron beam with fast rise and fall times.*

- *Are there microscopic mechanisms that are common to both the non-equilibrium plasma pinch and the equilibrium nearly DC-like discharge that may be exploited in the macroscopic/microscopic study of basic plasma pinch physics research?*

It is anticipated upon understanding the coupling mechanisms behind the plasma pinch, one may harness and control the copious products and by-products of the pinch as gases (charged and neutral) collapse upon and momentarily thermalize themselves until instabilities dominate resulting in a short pulse duration. A magnetic force driven plasma sheath is responsible for this collapse (pinch) and stagnation. Single fluid codes and theories tend to breakdown during these stages since the extraction of charges of one sign statistically violates quasi-neutrality or the statistical nature of interpenetrating fluids inherent in the models. Particle in cell codes and kinetic theory are complicated to implement since the pinched plasma is dense and constantly dynamic over time scales of interest. On a microscopic level it is also anticipated that the equilibrium nearly DC-like discharge and the non-equilibrium plasma pinch have some basic pinch mechanism similarities especially during the stagnation time of the non-equilibrium pinch. Experimentally and theoretically, this research endeavor takes a fresh look at the pinch mechanism and beam management issues for application driven plasma cathode high power microwave tube devices. The research is conducted in the Energy Materials Interaction Technology Initiative of Nevada (EMITION) Center at UNLV.

The grant in part supported: two graduate students Mr. Ahmad Al Agry and Sean Andersen; two high school teachers Mr. Chris Smith (two summers 2008 and 2009) and Mr. Thomas Bartling (summer 2008); two staff people Mrs. Shaoru Garner (partial support) and retiree Mr. Stan Goldfarb (nominal stipend per month); and in varying capacities, six undergraduate students. All participants in the research have, in varying degrees, gained practical experience with plasmas, laboratory equipment associated with the Non-Equilibrium Plasma Pinch (NEPP), high voltage and pulsed power technology, vacuum science and technology, data acquisition, and device and physics modeling. Nine out of the ten people supported by this grant are US citizens. The PI whom is also a US citizen is not considered in this count. Table 1 provides personnel names, positions, and their primary efforts towards the research initiative.

Table 1: Funded personnel associated with the research effort.

Personnel	Position	Effort
Shaoru Garner **(US)** [~Half Time Effort]	Research Associate (Full time staff researcher [MS Degree]	Funded on average approximately half time over the duration of the grant. She supported activities and continuity leading to lab preparation for the NEPP test stand, its operation, and redesign. This includes all of the ancillary equipment management required to perform experiments. Her efforts in this manner support a PhD graduate student. She also works with a nearly DC plasma discharge aiding a MS student research effort. She also participated in the high school teacher summer laboratory research experience. (Electrical Engineer)
Jackie Schill **(US)**[Hourly]	Undergrad. (less than nine month period part time hourly)	Artist and laboratory/data analysis engineer. Generated some 3D artwork of a conceptual NEPP for UNLV/KTech STTR and detailed artwork of the actual machine once built. Some of these works appear in this report and will appear in a future PhD thesis and paper. Also performed some data analysis studies. (Art and Computer Science)
Kris Buchanan **(US)**[Hourly]	Undergrad. – Army ROTC (Two months support)	Supported for less than two man months. Electrical and vacuum engineer. Currently attending graduate school in a US university. (Electrical Eng.)
Eduardo Olivares **(US)** [Hourly]	Undergrad. (6/30/10 – 5/1/11)	Floats where needed for experimentation. Major effort in PSpice modeling and simulation and in data analysis. *He has shown interest in attending graduate school at UNLV with my group.* (Electrical Eng.)
Julius Cervana **(US)** [Hourly]	Undergrad. (6/30/10 – 5/1/11)	Floats where needed for experimentation. Performs some simulation and modeling using Matlab, Kaleidagraph (data analysis tool), and PSpice. (Computer Eng.)
Luc Delgado **(US)** [Hourly]	Undergrad (6/30/10 – 5/1/11)	Floats where needed for experimentation. Major effort in PSpice and MATLAB modeling, simulation, and data analysis. (Electrical Eng.)
Wendell (Colby) Robinson **(US)** [Hourly]	Undergrad (5/10-9/10)	Computer modeling with PSpice of the high energy large electron beam population beam management device. (Electrical Eng.)
Sean Andersen **(US)**	Undergrad. Spring/Sum. 2010 ***MS Graduate Student: Fall 2010 to present***	**Undergraduate:** Electrical and vacuum engineer. Worked with high school teacher and undergraduate students in obtaining data from the plasma discharge tube experiment. **Graduate:** Sean joined the research center in Fall 2010 as a MS candidate. His research deals with the basic physics and application of a nearly DC plasma discharge tube for pinch studies. This work has a number of applications both internal and external to AFOSR.
Ahmad Al Agry (Visa)	***PhD Graduate Student***	Experimental, simulation, and theoretical efforts leading to basic research on the plasma pinch and to the application of the pinch as an electron source for high power microwave tube devices.
Stan Goldfarb **(US)**	Volunteer	Vacuum specialist in the retirement community – Helps train students in vacuum theory and technology. Works with vacuum systems and modifications to such systems. Constant source of information in vacuum technology, measurement, and in troubleshooting.

A brief timeline of the research is highlighted in bullet form. Also in bulleted form, outcomes are presented following the timeline. These are further elaborated on in the body of the final report. A concise bulleted timeline of the research endeavor is:

- Grant was received May 1, 2008. The grant supported people. Funds for experimentation were to be sought. We had promised to write a DURIP proposal for funds to build a suitable Non-Equilibrium Plasma Pinch (NEPP) for experimental studies.
- A AFOSR/UNLV High School Teacher Summer Laboratory Research Experience was conducted over the summer of 2008 with two teachers. The teachers examined a DC discharge phenomena with applications to NEPP. The purpose of their experimental work was to establish criteria needed for a more optimal NEPP especially in the take off-region of the pinch. A list of criteria was established. The work also identified a unique physical mechanism that was further investigated years later by the research group in conjunction with the grant.
- PhD candidate Mr. Ahmad Al Agry was identified as a suitable candidate for the research and was admitted in Fall of 2008 to begin his PhD degree supported by the grant.
- Mr. Agry was immersed in learning MAGIC and reviewing the recent literature on dense plasma foci.
- Mr. Agry independently developed a technique to calibrate the patented UNLV dots that exploits the device's capabilities and provides a calibration factor that relates the terminal voltage of the dot to the fields being measured. The calibration procedure has been further refined over the time duration from 2008 to 2011.
- An STTR announcement was released requesting non thermionic emission cathodes for high power microwave magnetrons. Under this announcement UNLV and KTech jointly submitted a proposal on 9/22/08 based on a very novel approach of coupling pulsed energetic electrons from the plasma pinch in a poor vacuum environment to a magnetron cathode in an ultra high vacuum environment.
- A High School Teacher Summer Laboratory Research Experience was conducted over the summer of 2009 with one teacher due to availability of external research funds outside of AFOSR. The teacher re-examined the nearly DC-like discharge phenomena but under a different venue addressing question "How does the ambient pressure affect the plasma discharge?"
- In September of 2009 an STTR award was received. By May 1, 2010, with some design input from UNLV, KTech built the UNLV NEPP. The UNLV PI transported the untested device to his lab from the New Mexico based company.
- Trigger circuitry was built and the device was tested in May and June 2010. After some seemingly successful shots, expensive gas switches were blown. Over the next six months after the STTR final report was written, the machine was reconfigured to distribute the energy in a more evenly manner among the gas switches upon fault conditions. Further, the UNLV trigger circuitry was redesigned. KTech collaborations were invaluable. Rogowski coil measurements indicate that the NEPP has exceptionally strong pinches.
- In parallel, Mr. Agry examined various beam focusing configurations to transport the electrons from the pinch through the beam drift tube to the magnetron cathode using the Magic particle-in-cell code.
- MAGIC was not accessible by summer of 2010.
- Using MAGIC when accessible and PSpice modeling, a unique beam management device was conceived without the need for a focusing magnetic field. A provisional patent was filed in May of 2011.
- Mr. Sean Andersen, whom worked with the research group for a year as an undergraduate student and then joined the research group as a MS candidate graduate student in Sept. 2010. He was intrigued with the nearly DC-like equilibrium discharge studies with its

application to the NEPP and other fields. He is currently pursuing the understanding of the microscopic mechanism responsible for the pinch characteristics in equilibrium both theoretically and experimentally. It is anticipated that the some of this study is of value in the sheath physics of the NEPP pinch.

- Special lectures on plasma physics pertinent to the dense plasma focus and one dimensional models of the dense plasma focus were prepared and delivered over a two month duration to students from Dec. 2010 to January 2011.
- Theoretical models for both the NEPP and the nearly DC-like equilibrium discharge have evolved over the past two years plus.
- A mock magnetron shell with beam management device have been designed, machined, and installed in the NEPP.

Research outcomes are

- Pulsed power calibration technique for patented EM dot sensors. [A. Al Agry, R. A. Schill, Jr., S. Garner, S. Andersen, and K. Buchanan, ***Electromagnetic Dot Sensor – Calibration***, **2009 17th IEEE Int. Pulsed Power Conf. (PPC 2009)**, Washington DC, June 28- July 2, 2009, pp. 1348-1353.]
- High energy, high electron population, magnetic free, beam management device and models [Patent Pending]
- Fully operational Non-Equilibrium Plasma Pinch (NEPP)
- Fully operational nearly DC-like plasma equilibrium discharge tube experiments
- A simple non-linear theory to describe the DC discharge has been developed. Currently, the paper is under preparation for journal submission: Sean Andersen and Robert A. Schill, Jr., ***Simple Nonlinear Theory for Electron Channeling***. The journal that the article is to be submitted to has not been decided as of yet.
- The theory and calibration technique for the EM dot sensor is currently under preparation for journal submission. The article citation under preparation is: : Ahmad Al Agry, Robert A. Schill, Jr., and Shaoru Garner, ***Electromagnetic Dot Sensor – Theory and Calibration*** **, Review of Scientific Instruments.**.
- The foundation of a multi-scale perturbation technique embedded in a multi-fluid theory to characterize the non-equilibrium plasma pinch has been developed. Consistency in formulation has been shown in zero order. This is a NON-equilibrium theory.

This report is divided into the following sections. Section II provides ancillary activities related to detection and/or transport of the electron beam and the plasma pinch. The Non-Equilibrium Plasma Pinch (NEPP) is presented in Sect. III. Experimental evidence of the pinch is provided. Section IV provides a zero-order multiple-scale, multi-fluid theory with suitable approximations for a NEPP device. The nearly DC-like discharge tube with experimental results is presented in Sect. V. Section VI highlights the theory that might help describe the physics in the equilibrium pinch. Section VII briefly describes the research activities of the high school teachers in their summer laboratory research experience. The report is concluded in Section VIII. Appendix A contains the slides and conference paper regarding the EM dot calibration presented in the PPC-2009.

II. EM Dot Sensor Calibration and Beam Management Device

EM Dot Sensor Calibration

A calibration test stand, one for B-dot mode and one for D-dot mode, and a calibration technique have been developed. The early development of this effort has been reported [A. Al Agry, R. A. Schill, Jr., S. Garner, S. Andersen, and K. Buchanan, ***Electromagnetic Dot Sensor – Calibration***, **2009 17th IEEE Int. Pulsed Power Conf. (PPC 2009)**, Washington DC, June 28- July 2, 2009, pp. 1348-1353.] Since 2009, the loading effects of the test stand and calibration technique have been significantly refined showing good agreement with theory. We are in the process of writing a peer review journal paper. Some highlights of the paper are presented below.

The UNLV patented EM dot if used appropriately allows one to measure the electric and magnetic fields it senses at one point in space simultaneously. Transient transitions between open circuit and short circuit states may be monitored on subnanosecond time scales. Dot calibration allows for absolute measurements of importance in characterizing both plasma pinch physics and electron production in the pinch. Figures 1a,b motivates a circuit model that includes test stand loading effects. The actual dot may be found in Fig. 1c.

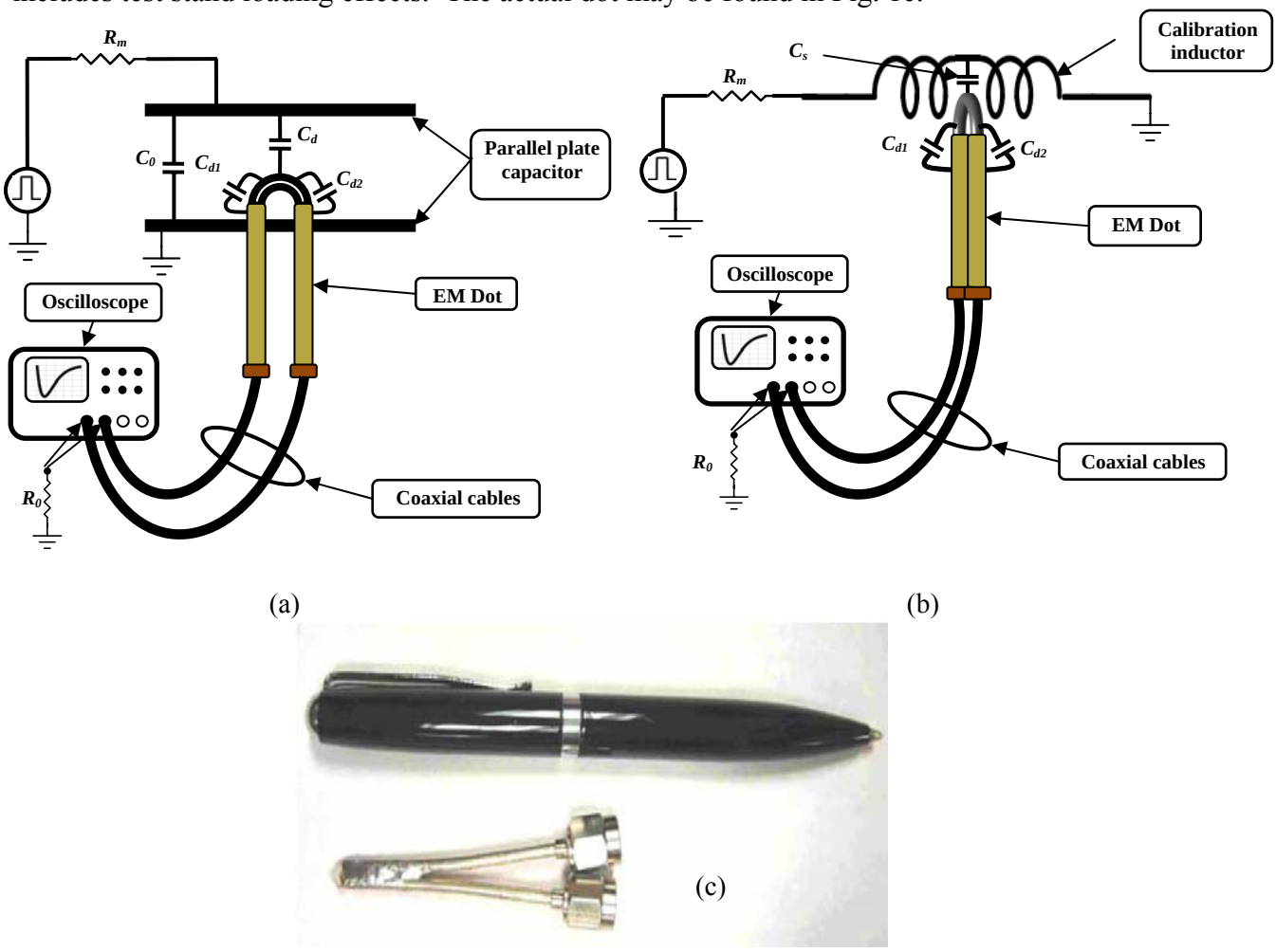

Fig. 1a-c. Cartoon schematic of EM dot in a a) D-dot test stand and b) B-dot test stand. Loading effects are partially illustrated using electrical components. c) The actual EM dot is displayed.

In the approximate theory, neglecting stray capacitance and inductance effects but retaining other test stand loading effects lead to the following source voltage driving the dot in

D-dot mode

$$V_s(t)=\left(1+\frac{R_m}{R_{12}}\right)\frac{(V_1+V_2)}{2}+\frac{1}{\tau_{12}}\int_0^t\frac{[V_1(t)+V_2(t)]}{2}dt+V_s(0)+ \\ +\tau_o\frac{d}{dt}\frac{[V_1(t)+V_2(t)]}{2}+\frac{\tau_o}{\tau_{12}}\frac{[V_1(t)+V_2(t)]}{2} \tag{1}$$

B-dot mode

$$V_s(t)=\frac{R_m}{M_c}\int_0^t[V_1(t)-V_2(t)]dt+[V_1(t)-V_2(t)] \tag{2}$$

in terms of the terminal voltages of the dot. These, in turn, may be appropriately related to the electric or magnetic field stimulus being measured. Here, V_1 and V_2 are the measured signal signatures, R_m is the resistance used for matching at the test stand, τ_{12}, τ_o, R_{12}, and M_c are respectively the time constants of the scope's loading effect on the coupling capacitance and the loading effect of the matching resistance on the coupling capacitance for the D-dot test stand, the loading effect of the oscilloscope for the D-dot test stand, and the mutual inductance coupling the test stand coil and the dot in the B-dot test stand. In the forth coming paper, we demonstrate that the loading effects of the test stands are negligible. Further, a general theory and code has been developed to incorporate loading effects of the experiment housing the sensor.

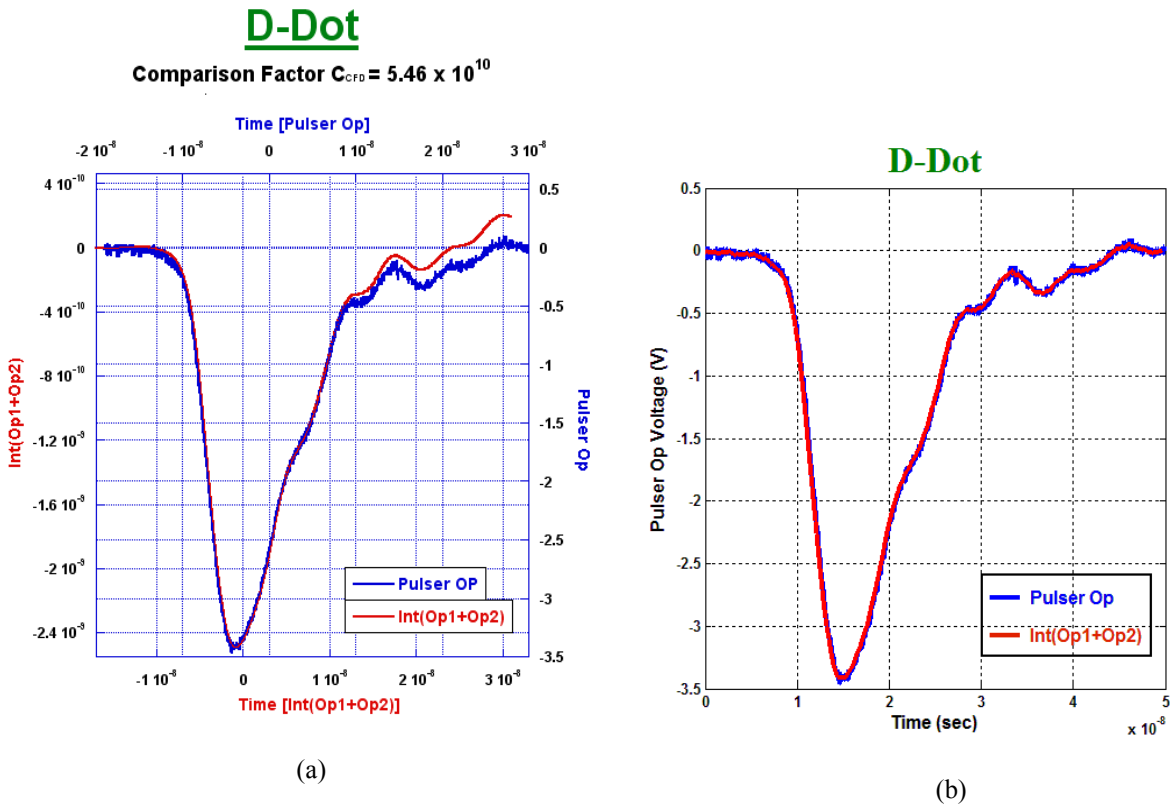

(a) (b)

Fig. 2a,b Calibration study fitting the data processed EM-dot signal to the output monitor signal of a Bournlea pulsed power supply for the case when measuring (a) the electric flux density directly linked to

charge accumulation and indirectly linked to voltage. The output voltage of the Bournlea pulsed power supply is 1.4 kV with a temporal pulse profile evident in the figures. In (b), the blue signal is the 51.8 dB attenuated signal signature of the pulsed power supply as measured at the oscilloscope. The red signal is the time integrated signal as measured in the low capacitance parallel plate capacitor (~2.2 pF) in shunt with a matching resistor multiplied by the comparison calibration factor C_{CFD}. The sensor tip of the EM-dot is inserted in between the capacitor plates just beyond the surface of the ground plate at the center of the ground plate. Some of the loop area may be exposed in between the plates. The dimensions of the air filled 2.2 pF capacitor are: 5 cm × 5 cm x 1 cm. In (b), the blue signal is the 51.8 dB attenuated signal signature of the pulsed power supply as measured at the oscilloscope. The red signal is the simulation result.

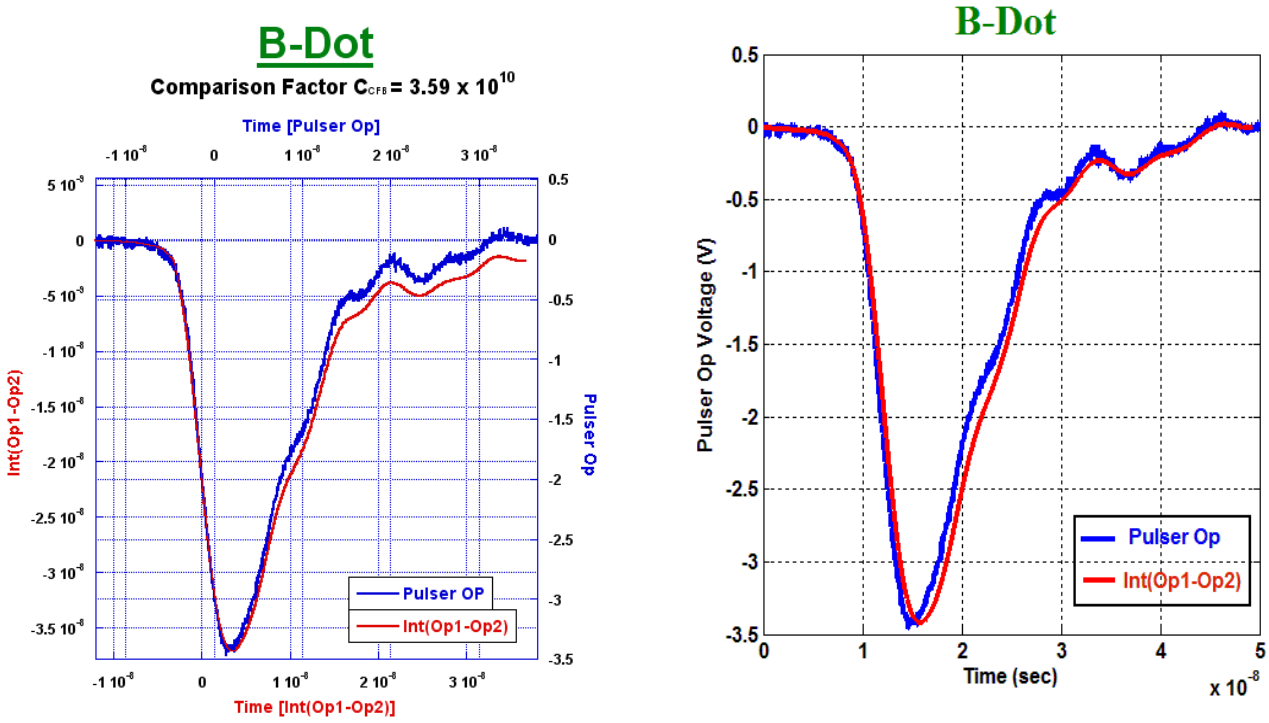

(a) (b)

Fig. 3a,b Calibration study fitting the data processed EM-dot signal to the output monitor signal of a Bournlea pulsed power supply for the case when measuring (a) the magnetic field directly linked to the output voltage of the Bournlea pulsed power supply is 1.4 kV with a temporal pulse profile evident in the figures. In (a), the blue signal is the 51.8 dB attenuated signal signature of the pulsed power supply as measured at the oscilloscope. The red signal is the time integrated signal as measured in the low inductance solenoid multiplied by the comparison calibration factor C_{CFB}. Here, the EM-dot is inserted in the center of a well characterized 4 turn inductor test stand. In (b), the blue signal is the 51.8 dB attenuated signal signature of the pulsed power supply as measured at the oscilloscope. The red signal is the simulation result.

Figures 2a and 3a compare the input voltage stimulus to the test stand to the appropriate time integrated measured signal. The loading effects of the test stand are minimal. It is observed that the EM dot sensor very closely tracks the voltage generated by the pulser. The codes developed to model the sensor in D-dot and B-dot mode given the input data of the pulser voltage are also in very good agreement with experiment as illustrated in Figs. 2b and 3b.

Beam Management Device

A one dimensional theory suggests that the lifetime of the pinch is on the order of 10 ns. During this time theory suggests that a 100 kA to 300 kA electron beam current may be extracted from the pinch with typically non-relativistic beam energies. These estimates are based on estimated thermalization properties of the pinch and first ionization potentials of the dense medium. MAGIC simulations as well as simplified theories indicated that magnetic lenses and electron channeling schemes to focus the beam in the beam drift tube for microwave generation are impractical and unattainable. A device to capture, transfer, and, if applicable, emit charge was developed without the need of a focusing field. Currently, the device is in the patent pending stage and therefore will not be fully described in this document. Figures 4a,b displays a poor man's prototype built at UNLV for sealed magnetron, plasma cathode studies. The purpose was to remove thermionic emission constraints in producing a burst of electrons at the cathode.

(a) (b)

Fig. 4a,b Illustration of a beam management device a) without and b) with the anode present.

The MAGIC modeling tool was used to study the properties of the device. Due to the inaccessibility of the code midway into the design process resulting from AFOSR budgetary issues, we developed a one dimensional PSpice code to model the physics of the beam management device. Although result differences do exist, the beam management device shows some promise to be verified through experimentation.

III. UNLV Non-Equilibrium Plasma Pinch (NEPP)

A Mather type dense plasma focus (DPF) like device denoted as a non-equilibrium plasma pinch (NEPP) was designed as an electron production device to source slow wave and cross-field high power microwave devices. The end objective was to use the electron source as a means to generate a burst of high power microwaves before pulse shortening instabilities destroy the properties of the beam. The microwave formation ambient environment could be a high or ultra-high vacuum environment or a low vacuum plasma environment. To this end, UNLV and

K-Tech Inc. was awarded an AFOSR STTR to design and build the UNLV NEPP. The experimental setup is shown Figs. 5a,b. The device consists of a solid anode surrounded by a cage consisting of 16 rods which acts as the cathode. Refer to Figs. 6a,b in particular Fig. 6b. The length of the anode is 28 cm and the radius is 3.7 cm. The length of the cathode is 36.5 cm and the radius is 6.4 cm. Potentially, the filling gas inside the chamber will be either hydrogen or helium. The optimal chamber pressures range between 1 and 10 Torr. A capacitor bank consists of fifteen 5 μF capacitors charged in a parallel configuration (total capacitance of 75 μF). The charging voltage ranges between 15 and 20 kV using a high voltage (HV) power supply. Respectively, the capacitors then release energy between 8.4 kJ and 15 kJ to the electrodes symmetrically through a radial transmission line (RTL) by way of high voltage spark-gap gas switches to drive the plasma pinch, as shown in Fig. 6a. A second HV power supply energizes a transmission line system used to trigger spark-gap switches. Refer to Fig. 5a.

In the original design, each of the six spark gap gas switches were connected to all fifteen capacitors in a parallel configuration by way of a solid annular ring. To reduce the risk of damaging the spark gap switches resulting potentially from switch pre-fire, the ring that is attached to the fifteen capacitors has been divided into three equal sections separated with a 2 cm air gap and ends wrapped in Mylar insulation to prevent breakdown. Therefore, each section consists of five capacitors and two spark gap switches. In case of pre-fire, only one third of the entire capacitor bank energy (the energy of five capacitors) will pass through the spark gap switch instead of the energy of the whole capacitor bank, as depicted in Fig. 7. Under normal operation all spark gap switches fire simultaneously each releasing one-sixth of the bank energy symmetrically to the radial transmission line and finally to the load at the end.

Currently, the test stand chamber houses an ultra pure 1 Torr helium environment. Helium and hydrogen environments have been partially characterized in the NEPP. The helium environment has consistently shown strong pinch effects as identified by Rogowski coil measurements. With a 75 μF capacitor bank charged to 15 kV, a one dimensional theory predicts the sheath current in the pinch as displayed by the dashed line in Fig. 8a. The fast drop at the normalized time of 1.95 on the graph is a consequence of the pinch. The one-dimensional code crudely characterizes the pinch. The Rogowski coil detects the rate of change in current or equivalently rate in change in the magnetic field be means of induction as depicted by the red line in Fig. 8b. The blue curve shown in Figure 8b is the time integrated signal, namely the NEPP test stand current supplying the plasma pinch. The drastic change in current (blue line) occurring at about 2.5 μs is the sign of a significant pinch. We are approaching ~25-40% current drop between end of rundown stage and pinch stage. The rundown (or acceleration) stage time is about half of the predicted time. Since the one dimensional code does not take into consideration the take-off stage of the pinch and the shortened anode due to the glass insulator, the predications are reasonable.

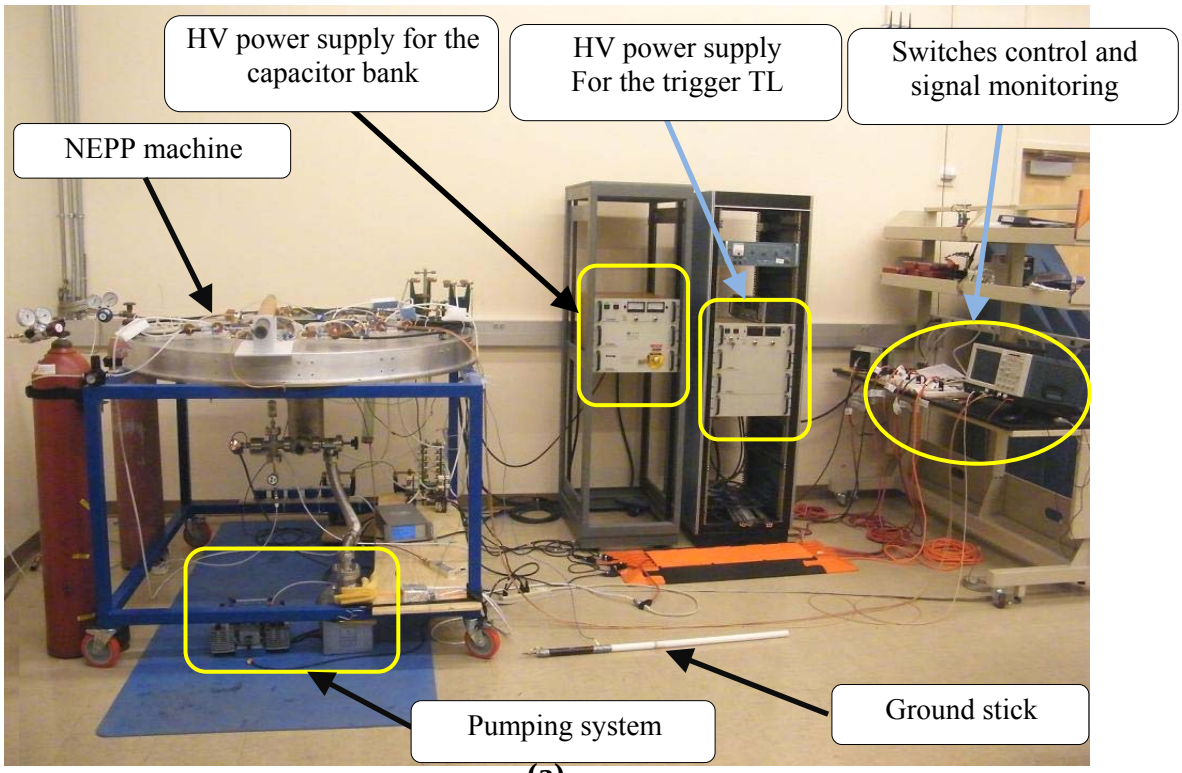

(a)

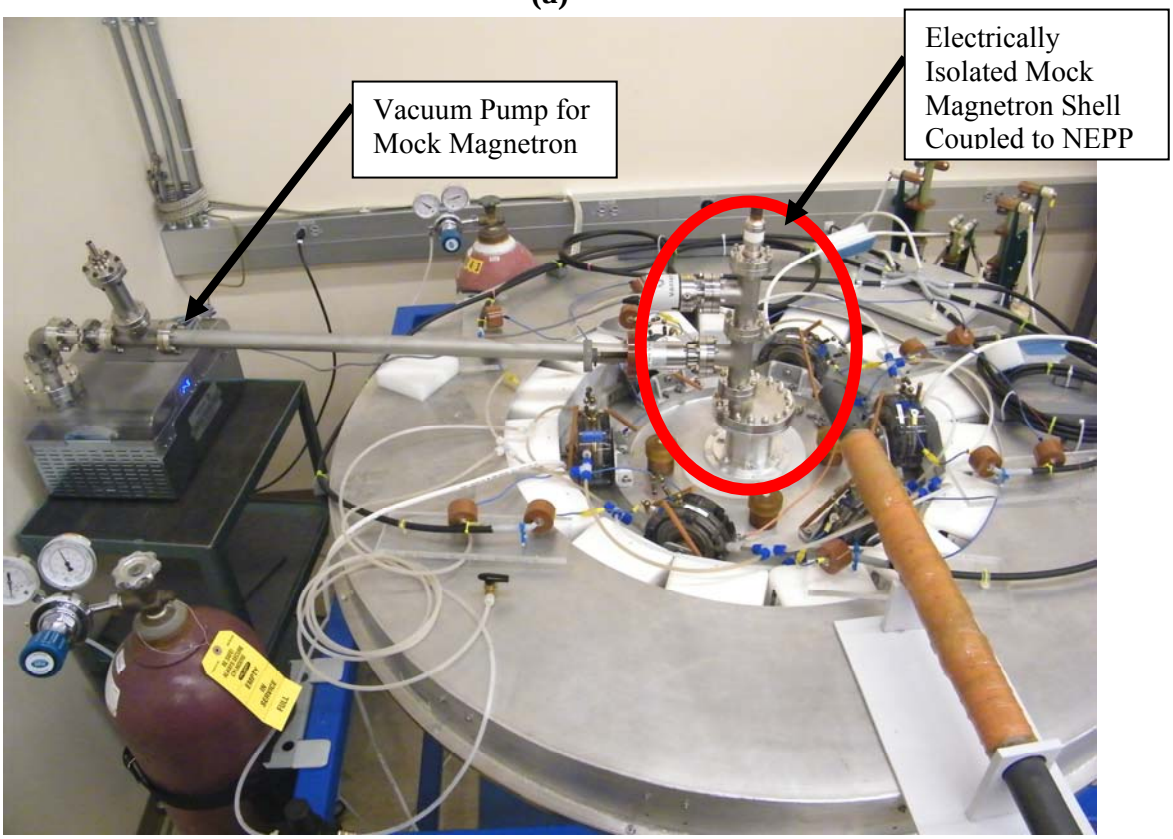

(b)

Fig. 5a,b a) Overview of the UNLV NEPP experimental setup in the absence of the mock magnetron shell. b) Mock magnetron shell with associated vacuum plumbing coupled directly to the NEPP.

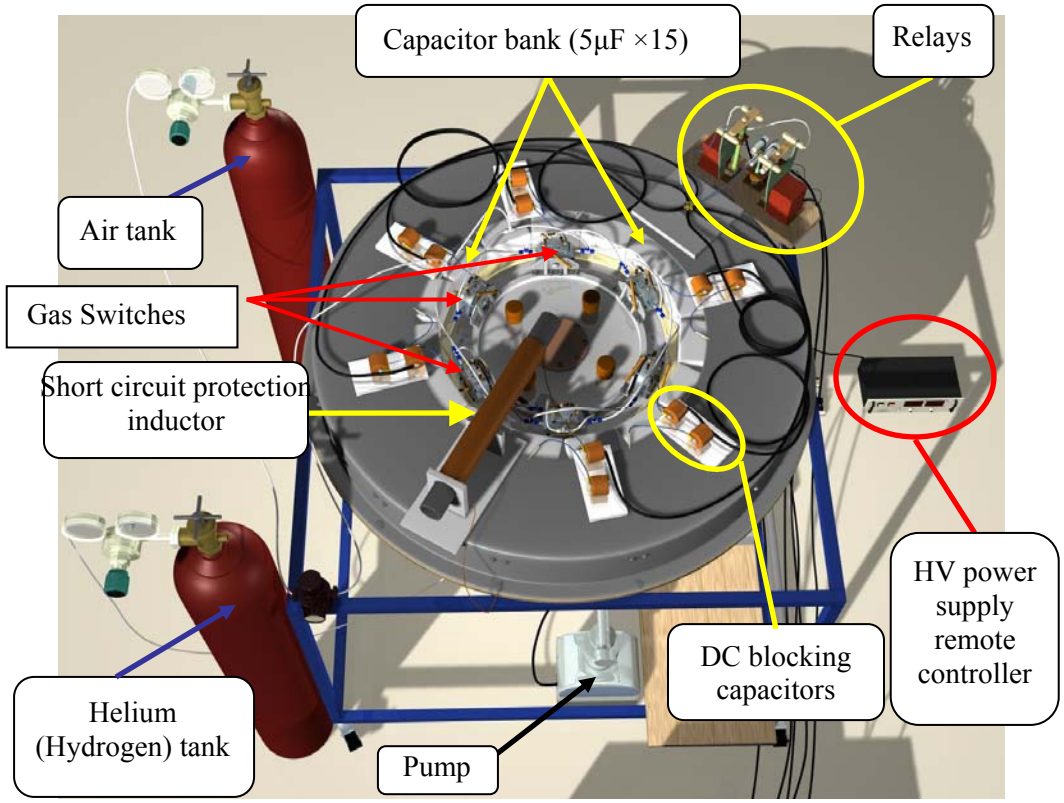

(a)

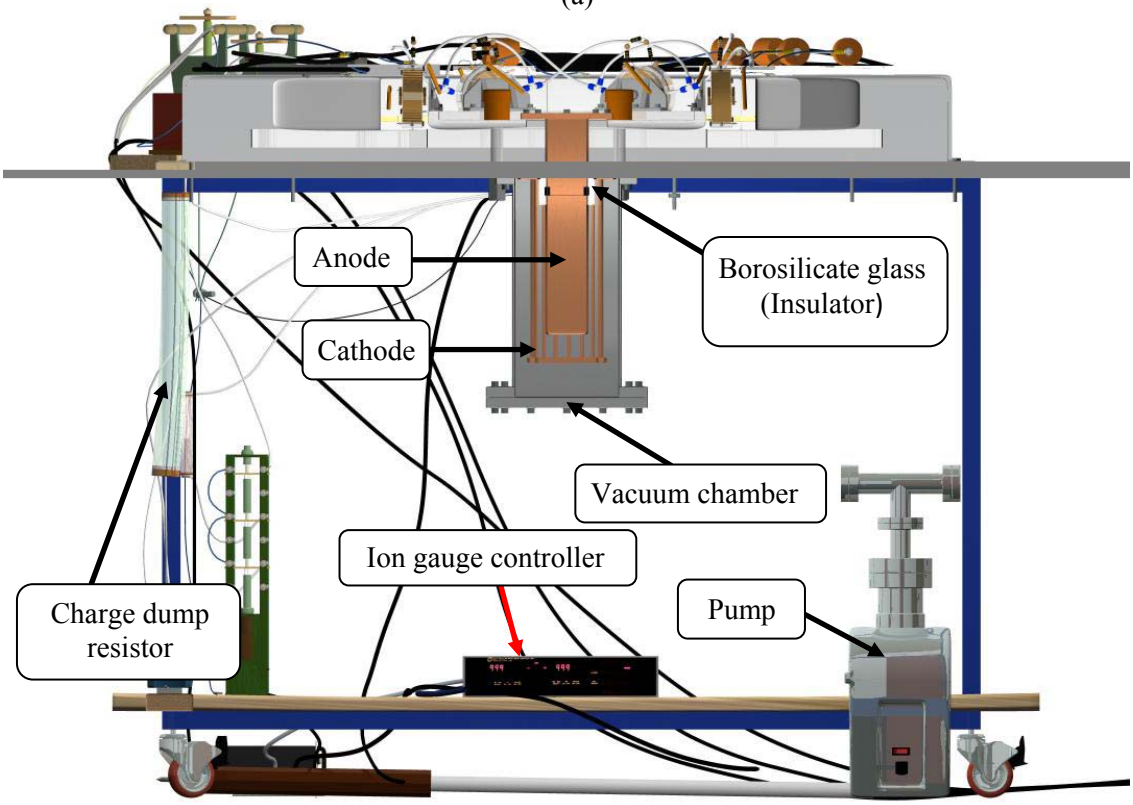

(b)

Fig. 6a,b UNLV NEPP machine. (a) Top view, and (b) cross-sectional view

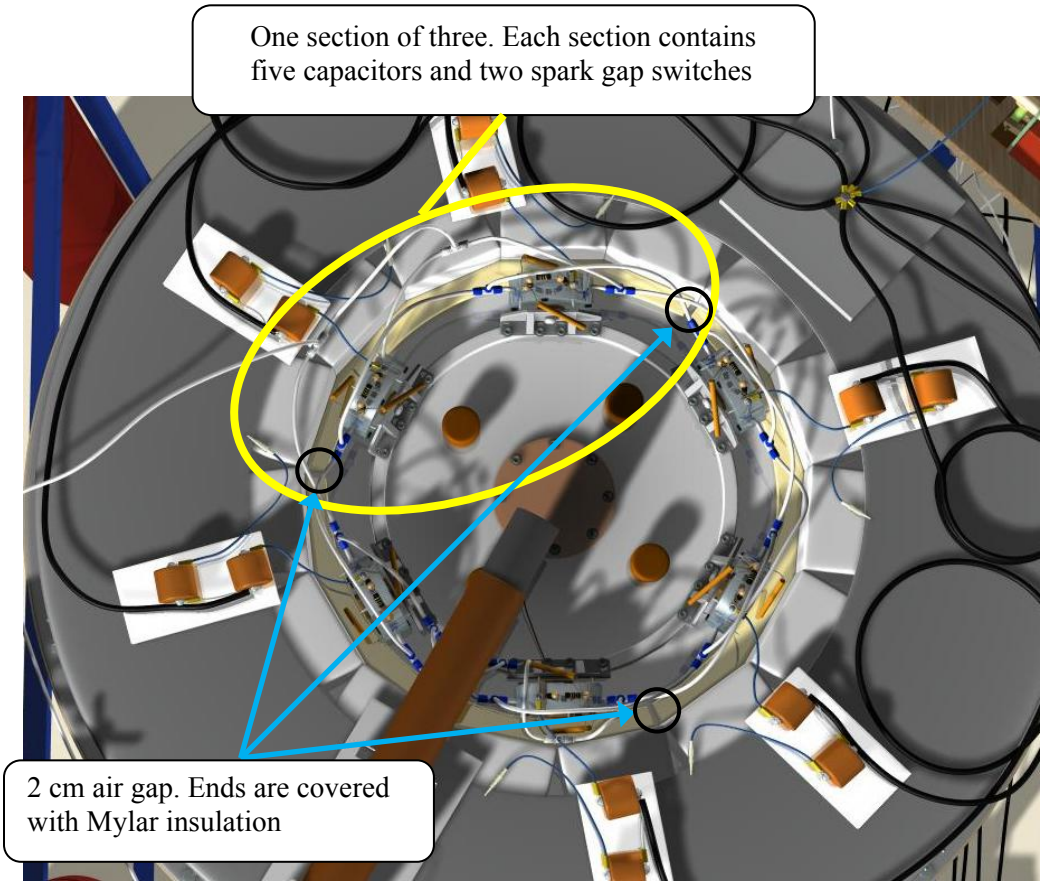

Fig. 7 Top view shows the air gap between each section.

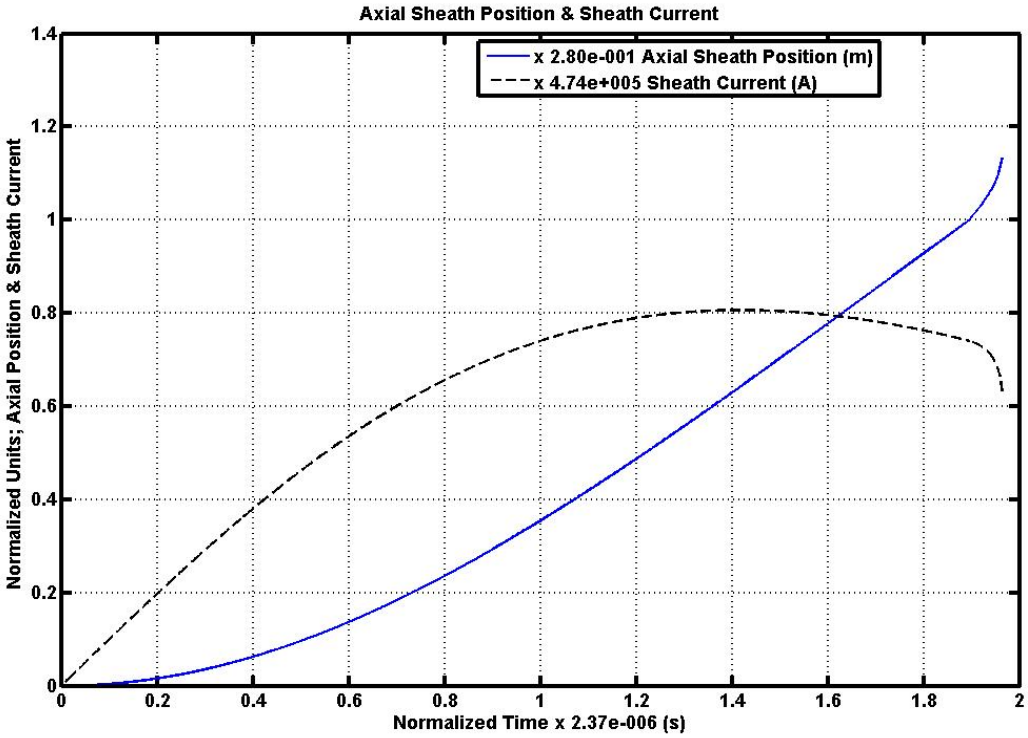

(a)

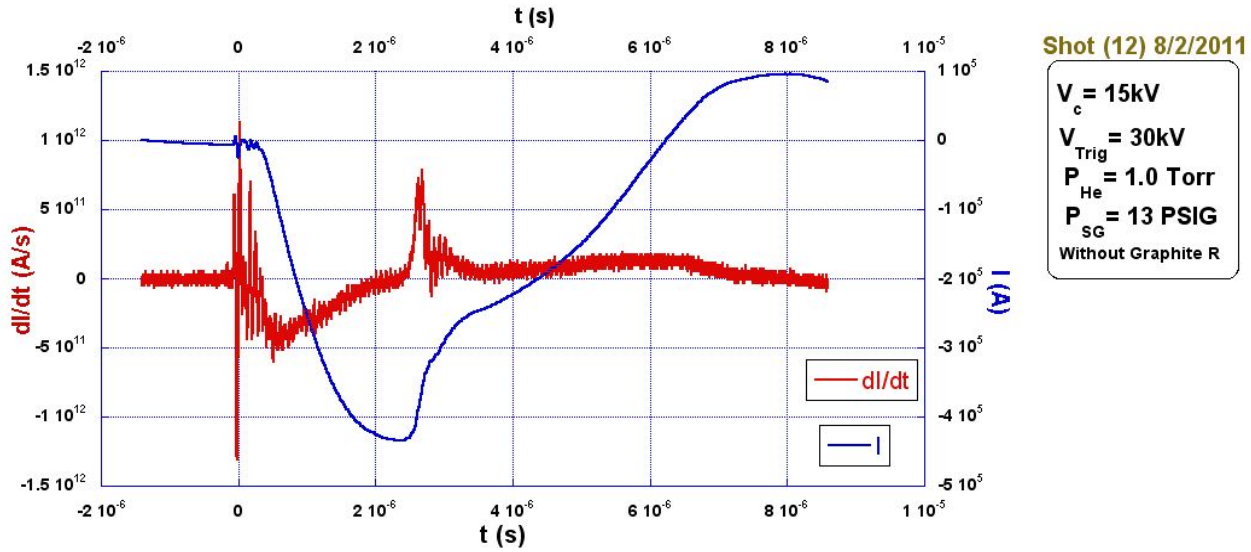

(b)

Fig. 8a,b (a) Predicted and (b) experimental current contained in the sheath in the axial and compression stage of the plasma pinch.

Figure 9 displays an assembly view of the mock magnetron pictured in Figs. 4a,b. The cavity dimensions and cathode dimensions are typical of a high power magnetron source. The objective is to measure the electron current transported to the cathode from the plasma pinch.

.

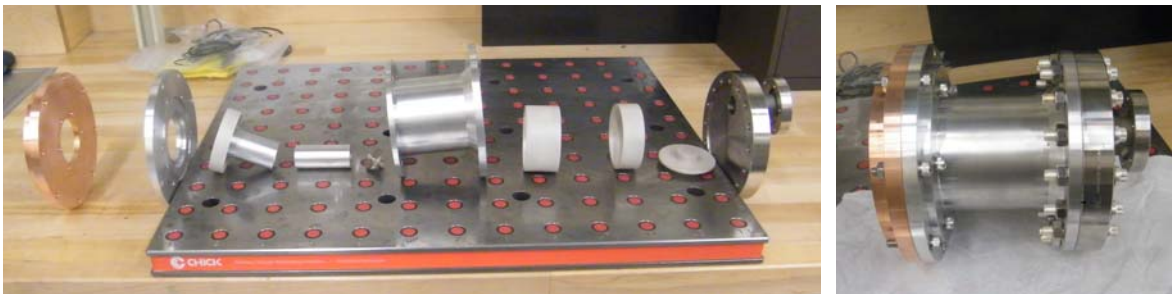

Fig. 9 Assembly display and assembled mock magnetron casing for testing the plasma cathode.

IV. Pinch Physics - Zero Order Theory

One of the goals of this research endeavor is to understanding the physical mechanism behind the plasma pinch leading to electron production. We have developed a theoretical platform making use of an unconventional multiple-scale technique with the plasma transport equations to characterize the non-equilibrium pinch properties. The plasma fluid is treated as a multi-fluid species subject to a weighted statistical test validating the fluid approximation.

The governing multi-fluid transport equations, connecting Maxwell's equations, and connecting circuit equations characterizing the plasma pinch are, respectively,

Mass Transport Equation:

$$\frac{\partial n_j}{\partial t} + \vec{\nabla} \cdot \left(n_j \vec{v}_j \right) = S_j, \quad j = e, i, n \tag{3}$$

Momentum Transport Equation:

$$m_j n_j \left[\frac{\partial \vec{v}_j}{\partial t} + \left(\vec{v}_j \cdot \vec{\nabla} \right) \vec{v}_j \right] = q_j n_j \left(\vec{E} + \vec{v}_j \times \vec{B} \right) - \vec{\nabla} p_j + \vec{A}_j - \vec{v}_j S_j, \tag{4}$$

Energy Transport Equation:

$$\frac{D}{Dt}\left(\frac{3 p_j}{2} \right) + \frac{3 p_j}{2} \vec{\nabla} \cdot \vec{v}_j + \left(\vec{\vec{P}}_j \cdot \vec{\nabla} \right) \cdot \vec{v}_j + \vec{\nabla} \cdot \vec{q}_j = M_j - \vec{v}_j \cdot \vec{A}_j + \frac{1}{2} v_j^2 S_j \tag{5}$$

Maxwell's Equations:

$$\vec{\nabla} \times \vec{E} = -\frac{\partial \vec{B}}{\partial t} \tag{6}$$

$$\vec{\nabla} \times \vec{B} = \mu_0 \left(n_e q_e \vec{v}_e + n_i q_i \vec{v}_i + \varepsilon_0 \frac{\partial \vec{E}}{\partial t} \right) \tag{7}$$

$$\varepsilon_0 \vec{\nabla} \cdot \vec{E} = n_e q_e + n_i q_i \tag{8}$$

Circuits Equation:

$$V_c(t) = L_0 \frac{di(t)}{dt} + i(t) R_0 + L_c(t) \frac{di(t)}{dt} + i(t) \frac{dL_c(t)}{dt} + i(t) R_{ps} + i(t) R_c(t) + L_D(t) \frac{di(t)}{dt} + i(t) \delta \frac{dL_D(t)}{dt} \tag{9}$$

and ancillary equations (charge density and current density)

$$\rho = n_e q_e + n_i q_i \tag{10}$$

$$\vec{J} = n_e q_e \vec{v}_e + n_i q_i \vec{v}_i \tag{11}$$

where space and time functional dependence $(\vec{r}, t)$ is implied on all field and fluid species characteristics. The circuit equation, Eq. (9), refers to the circuit model given in Fig. 10 relating the transformer and motional effects of the acceleration stage and in part the radial compression stage of the pinch to the external capacitor bank source and loading effects. The quantities above are defined as: *j=e, i*, and *n* respectively referring to the electron, ion, and neutral species; m_j and q_j are the species mass and charge respectively; n_j is the species number charge density; v_j is the species velocity; S_j is the collision term that characterize the rate of ionization, recombination or attachment of the jth fluid species with a different fluid species; $\vec{A}_j$ denotes the rate of change of the mean momentum per unit volume due to collisions between the jth fluid species with a

different fluid species; $\vec{E}(\vec{r},t)$ and $\vec{B}(\vec{r},t)$ are respectively the vector electric field intensity and vector magnetic flux density; ε_0 and μ_0 are the free space permittivity and permeability respectively; p_j is the species pressure; $\vec{\vec{P}}_j$ is the total kinetic pressure dyad; $\vec{q}_j$ is the heat flux density vector; and M_j is the rate of energy density transfer due to collisions of the jth specie with a different fluid species.

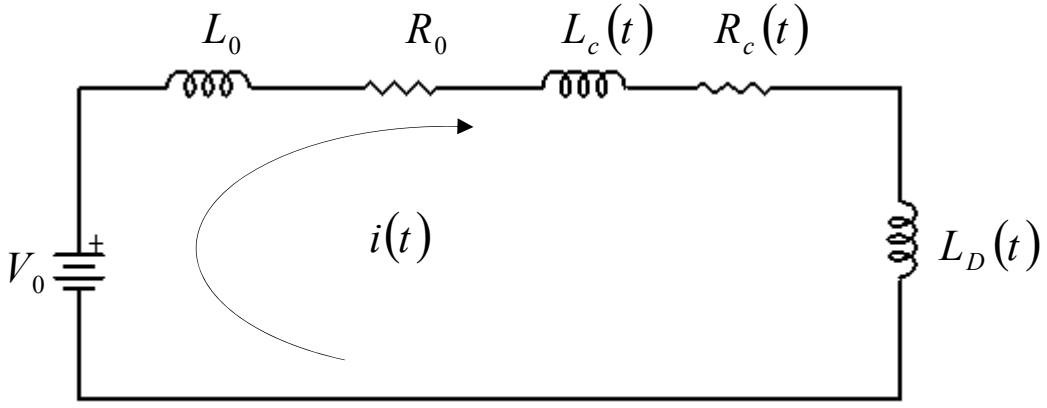

Fig. 10 Circuit model for the sheet dynamics in the NEPP.

Under appropriate conditions unique to the non-equilibrium plasma pinch in pinch mode based on a rigid, radial, sheet current plasma sheath model assuming that the transport of heat is negligible in lowest order, the following zero order *non-equilibrium* relations may be written as

Sheath Density:

$$n_{j0}(\vec{r},t) = -\frac{I_0\left(\tilde{\vec{r}},\tilde{t}\right)}{2\pi q_j r_0 v_{er0}\left(\tilde{\vec{r}},\tilde{t}\right)}\delta\left(z_{j0} - z_{ja} - \int v_{jz0}(\vec{r},t)dt_0\right) \tag{12}$$

Continuity Equation:

$$n_{js0}\left(r,\tilde{z},\tilde{t}\right)v_{jr0}\left(\tilde{r},z,t\right) = \frac{C_1\left(\tilde{r},z,t\right)}{r_0} \tag{13}$$

Electric and Magnetic Fields:

$$\vec{B}_0(\vec{r},t) = \mu_0\vec{H}_0(\vec{r},t) = \mu_0 H_{\varphi 0}(r,\varphi,z,t) = \frac{\mu_0 I_0\left(\tilde{\vec{r}},\tilde{t}\right)}{2\pi r_0}U\left(-z_{j0} + z_{ja} + \int v_{jz0}(\vec{r},t)dt_0\right) \tag{14a}$$

$$E_{r0}(\vec{r},t) = \frac{\mu_0 I_0\left(\tilde{\vec{r}},\tilde{t}\right)v_{jz0}(\vec{r},t)}{2\pi r_0}U\left(-z_{j0} + z_{ja} + \int v_{jz0}(\vec{r},t)dt_0\right) \tag{14b}$$

Scalar Hydrostatic Pressure:

$$p_{jr0}(\vec{r},t) = p_{jsr0}(r,\tilde{\varphi},\tilde{z},\tilde{t})\,\delta\left(z_{j0} - z_{ja} - \int v_{z0}\,dt_0\right) \tag{15a}$$

$$p_{jz0}(\vec{r},t) = p_{jz0a}(r,\tilde{\varphi},\tilde{z},\tilde{t})\,U\left(z_{ja} + \int v_{jz0}\,dt_0 - z_{j0}\right) - p_{jz0b}(r,\tilde{\varphi},\tilde{z},\tilde{t})\,U\left(z_{j0} - z_{ja} - \int v_{jz0}\,dt_0\right) \tag{15b}$$

Space Charge Electric Field:

$$E_{ze0}(\vec{r}_j,t) = -\frac{b\tilde{\rho}_{ks0}(\tilde{\vec{r}}_k,\tilde{t})}{4\pi\varepsilon_0}\hat{z}\int_a^b\int_0^{2\pi}\frac{(z_{j0}-z_{k0})}{\left[r_{j0}^2 + r_{k0}^2 - 2r_{k0}r_{j0}\cos(\varphi_{j0}-\varphi_{k0}) + (z_{j0}-z_{k0})^2\right]^{3/2}}\,dr_{k0}\,d\varphi_{k0} \tag{16}$$

Momentum Transport Equations

$\hat{r}$:

$$m_j n_{sj0}(r,\tilde{z},\tilde{t})\left[\frac{\partial v_{jr0}(\tilde{r},z,t)}{\partial t_0} + v_{jz0}(\vec{r},t)\frac{\partial v_{jr0}(\tilde{r},z,t)}{\partial z_0}\right] = -\frac{1}{r_0}\frac{\partial}{\partial r_0}\left[r_0 p_{jsr0}(r,\tilde{\varphi},\tilde{z},\tilde{t})\right] \tag{17a}$$

$\hat{z}$:

$$m_j n_{js0}(r,\tilde{z},\tilde{t})\left[\frac{\partial v_{jz0}(\vec{r},t)}{\partial t_0} + v_{jz0}(\vec{r},t)\frac{\partial v_{jz0}(\vec{r},t)}{\partial z_0} + v_{jr0}(\tilde{r},z,t)\frac{\partial v_{jz0}(\vec{r},t)}{\partial r_0}\right] =$$

$$q_j n_{js0}(r,\tilde{z},\tilde{t})\left[E_{kz0}(r,\tilde{\varphi},z,t) + \frac{v_{jr0}(\tilde{r},z,t)\mu_0 I_0(\tilde{\vec{r}},\tilde{t})}{2\pi r_0}\right] - \left[p_{jz0a}(r,\tilde{\varphi},\tilde{z},\tilde{t}) - p_{jz0b}(r,\tilde{\varphi},\tilde{z},\tilde{t})\right] \tag{17b}$$

Current density:

$$J_r(\vec{r},t) = \frac{I_0(\tilde{\vec{r}},\tilde{t})}{2\pi r_0}\,\delta\left(z_{j0} - z_{ja} - \int v_{jz0}(\vec{r},t)\,dt_0\right) \tag{18}$$

Circuit Equation:

$$V_{co}(t) = V_o = i_o(\tilde{t})R_0 + i_o(\tilde{t})R_{ps} \tag{19}$$

Energy Transport Equation (based on an added assumption that the velocity and pressure over the sheath disk is independent of radius in lowest order implying that the disk shape is not canted in lowest order) :

$$p_{jsro}(r,\tilde{\varphi},\tilde{\vec{z}},\tilde{t}) = -\frac{r_0}{2}\frac{v_{jz0}(\tilde{r},z,t)}{v_{jr0}(\tilde{r},z,t)}\left[p_{jz0a}(\tilde{\vec{r}},\tilde{t}) - p_{jz0b}(\tilde{\vec{r}},\tilde{t})\right] + \frac{K(\tilde{\vec{r}},\tilde{t})}{r_0} \tag{20}$$

Equation of State (or is a small term in lowest order):

$$\vec{\nabla}_o \cdot \vec{q}(\tilde{\vec{r}},\tilde{t}) = 0 \tag{20}$$

where $C_1(\tilde{r},z,t)$ and $K(\tilde{\vec{r}},\tilde{t})$ are constant in the lowest order variation of the radius. In the spirit of the multiple-scale technique, $f(x,t)=f(x_0,x_1,x_2,\ldots,t_0,t_1,t_2,\ldots)=\delta^0 f_0+\delta^1 f_1+\delta^2 f_2+\cdots$ where the ~ superscript notation on $\vec{r}$ and/or t is used to imply that $(\tilde{\vec{r}},\tilde{t})=(\vec{r}_1,\vec{r}_2,\vec{r}_3,\ldots,t_1,t_2,t_3,\ldots)$ that a function is independent of the lowest order in space and/or time scale.

The lowest order relations are self-consistent and describe the plasma characteristics in the pinch region. Typically, one may think of the modeled accelerated plasma in the acceleration stage continues its motion in the radial compression pinch stage in lowest order. The compression nature of the pinch is afforded in the next order with correction terms to the lowest order. Secular terms, terms that grow and become singular, are forced to zero which in turn provides a set of conditions which one can use to characterize the pinch mechanism. The solution to the zero and first order equations are currently being pursued.

V. Nearly DC-Like Discharge Tube

The nearly DC-like equilibrium discharge exhibits a stable physical phenomenon that may offer insights to pinch physics, thermalization, and stagnation (temporary stagnation) in the non-equilibrium plasma pinch (NEPP). Theoretical models to describe the stabilization of the discharge observed will be presented in the next section and are currently being explored experimentally. Figures 11a-c display the experimental set-up. Figure 11c, illustrates the means in which the discharge tube is sourced. The specifics on the experimental set-up are provided in Table 2.

Table 2. Measurable data on the discharge tube and parameters leading to data presented in Fig. 13. Typical experimental data ranges are provided.

Parameter	**Measurable**
Diameter of plate electrodes	4”
Distance of separation between plate electrodes	1.5”
Diameter of plastic discharge tube wall	8”
R_S	5.4 MΩ
C_0	50 nF
Pressure (1-20 Torr typical)	8.2 Torr
R_b (Typical 506 or 336 Ω)	506 Ω
Gas environment	Nevada Air

Figure 12a displays a typical discharge with six yellow sampling contours for image processing. With the aid of image processing codes, the intensity distribution of the emitted light is plotted along the contours. Figure 12b displays the light intensity along one of the contours passing radially through the discharge. By analyzing the spatial intensity of the discharge light, one may indirectly estimate the spatial profile of the plasma density along/across the discharge. Interestingly, a Gaussian curve (red) is fitted to the data. The light intensity (relative to the sensitivity of the camera) is displayed on the vertical axis. The horizontal axis is the pixel number and hence spatial parameter along the contour used to sample the image properties. Figures 13a-e present the data of a particular discharge as indicated in Table 2. Figures 13a,b

have not been electronically changed in size. Therefore, a one-to-one correlation exists in spatial location. The intense blue/purple light in the shape of a thin disk on the left of the picture over the electrode is the negative glow region. The negative glow region covers about 1/3 of the plate and is very thin. The negative glow does not appear to significantly migrate around the plate and is located away from the edges of the plate where field enhancement typically exists. The faded purplish glow to the right of the picture is the positive plasma column. Figures 13c-e provides the electrical properties of the discharge based on the source network provide in Fig. 11c. As anticipated, the voltage at the electrodes build up until breakdown occurs, the voltage of both the source and tube decreases. The both the initial surge of current and the rate of change in current are significant. Along with pressure considerations, these studies tend to suggest that the current and processes associated with the current are responsible for the stable cylindrical-like formation of the pinch. Indications suggest that electron channeling may be one physical mechanism that can explain the stability of the pinch in the discharge.

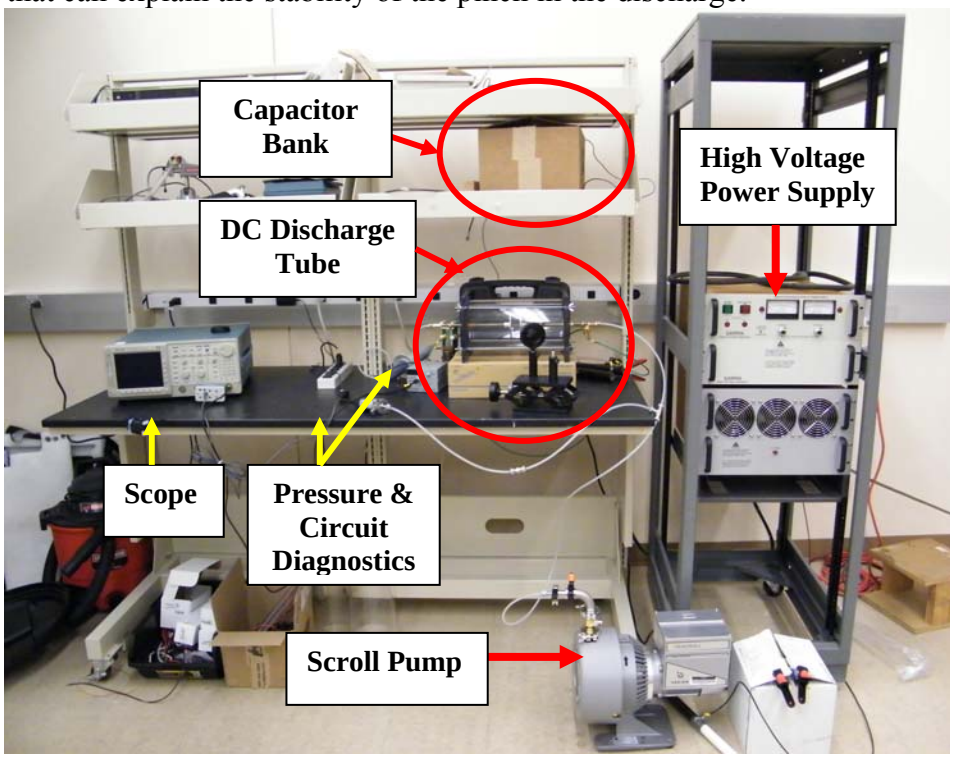

(a)

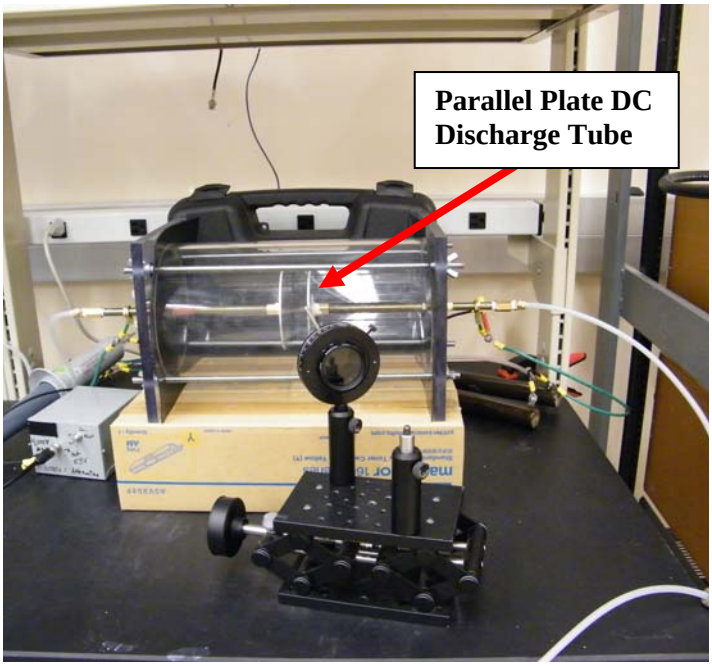

(b)

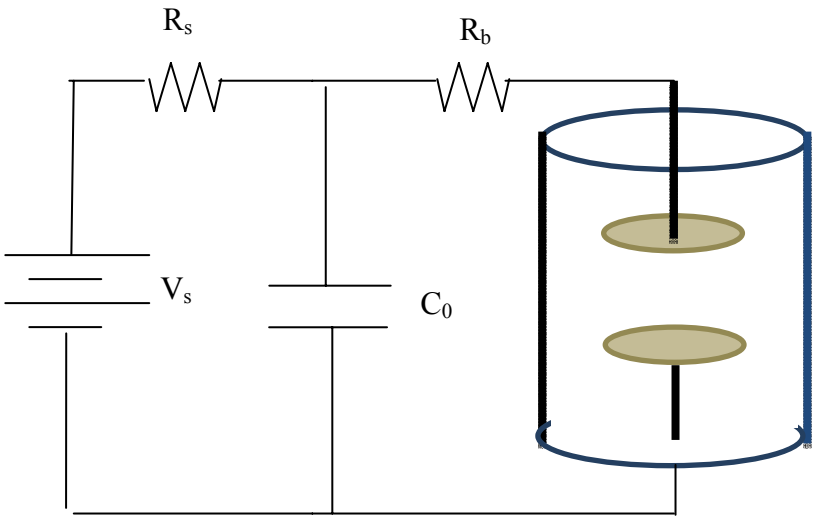

(c)

Fig. 11a-c The experimental setup of the nearly DC-like discharge tube displaying an a) overview of the experiment and b) the discharge tube with polarizer and camera mount. The electrical system energizing the discharge is shown in (c).

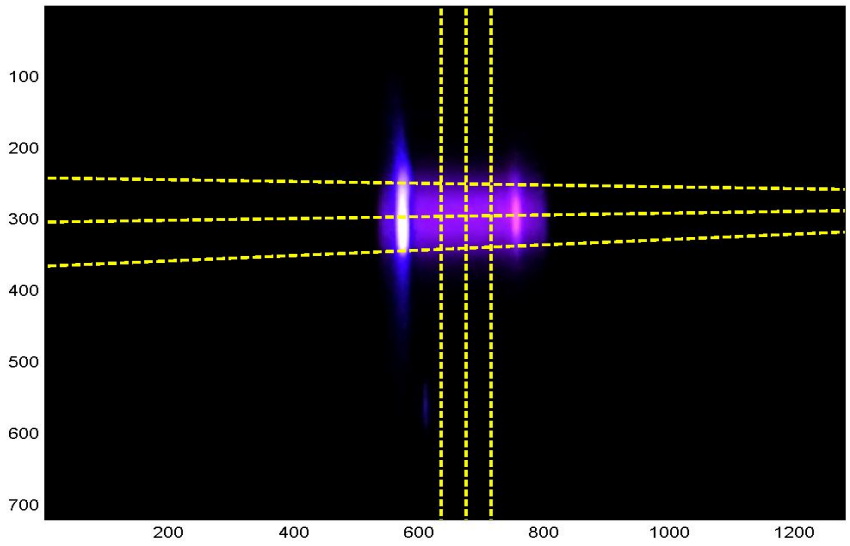

(a)

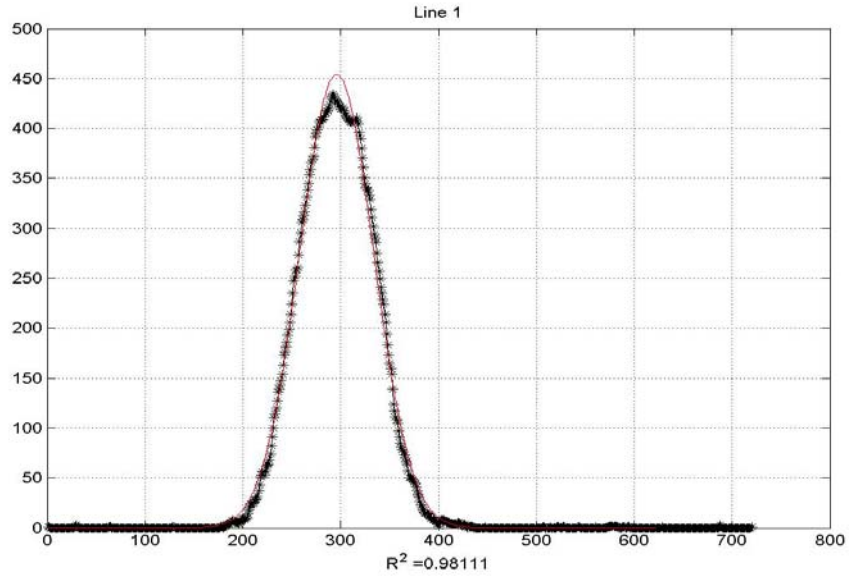

(b)

Fig. 12a,b A typical DC-like discharge is pictured in (a). The intensity of the discharge through one radial cross-section suggests information leading to the plasma density profile. A Gaussian curve (solid red line) is fitted to the data. The discharge is nearly constant in space and intensity but exhibits an on-off pulse like signature.

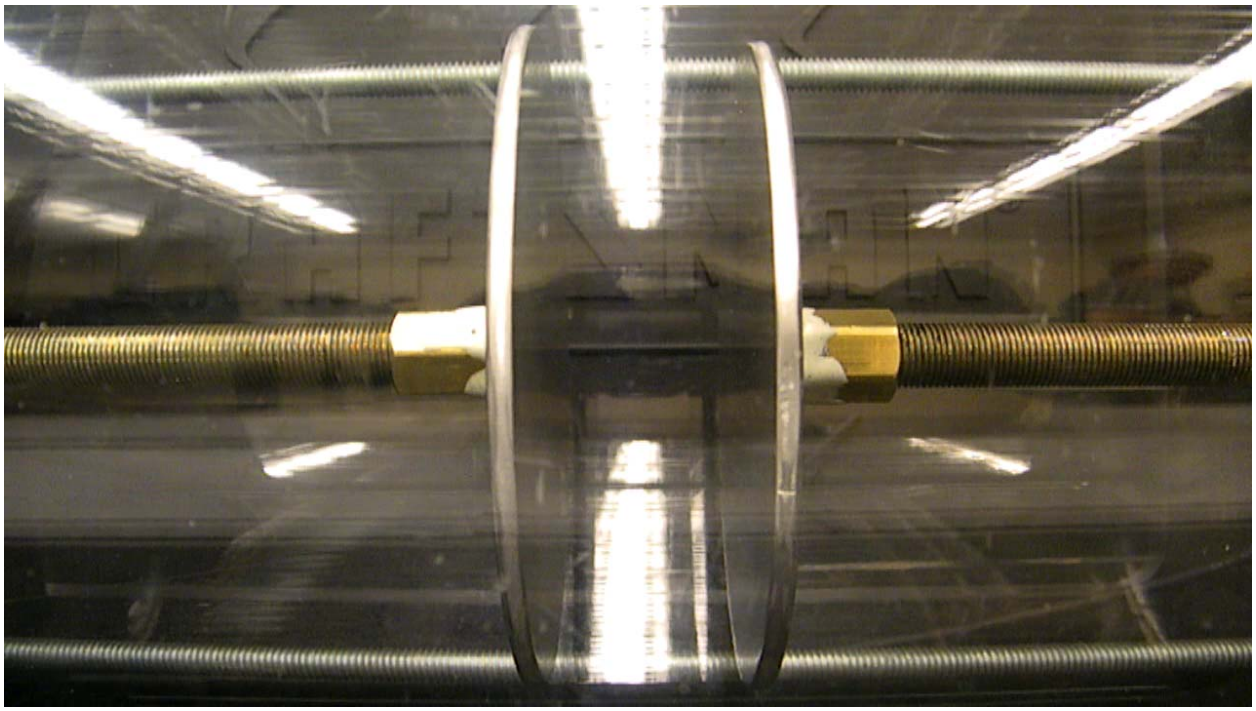

(a)

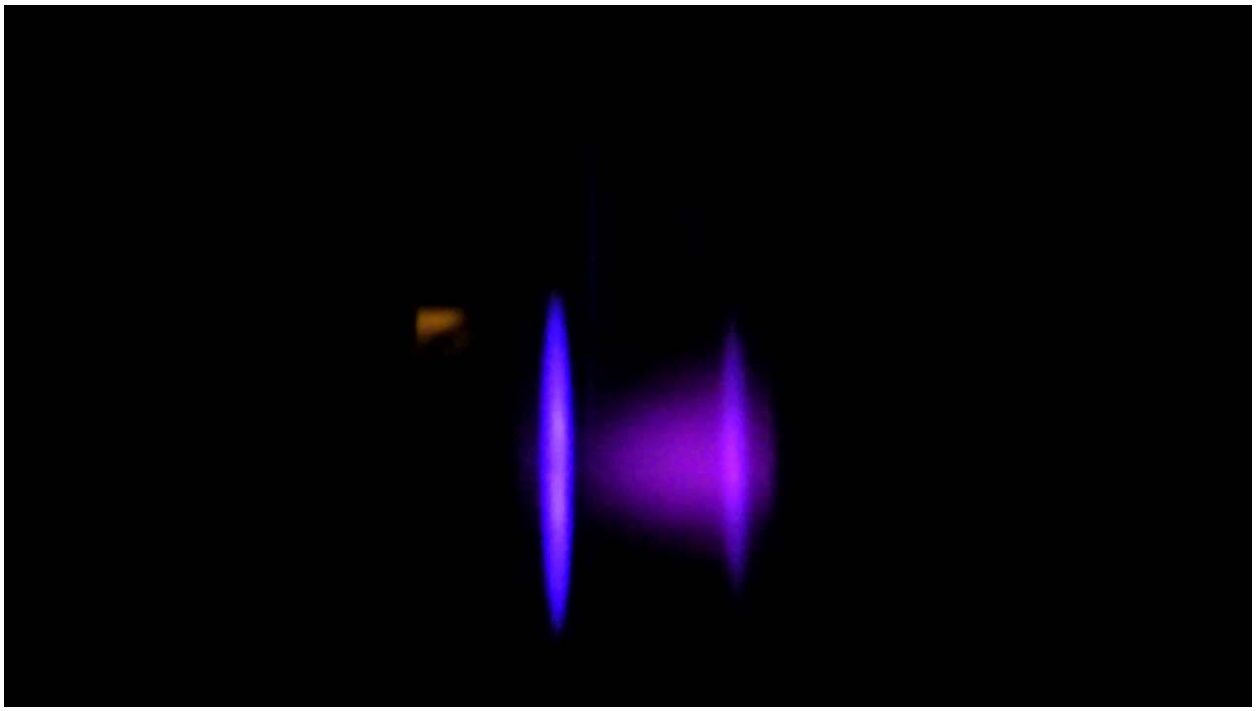

(b)

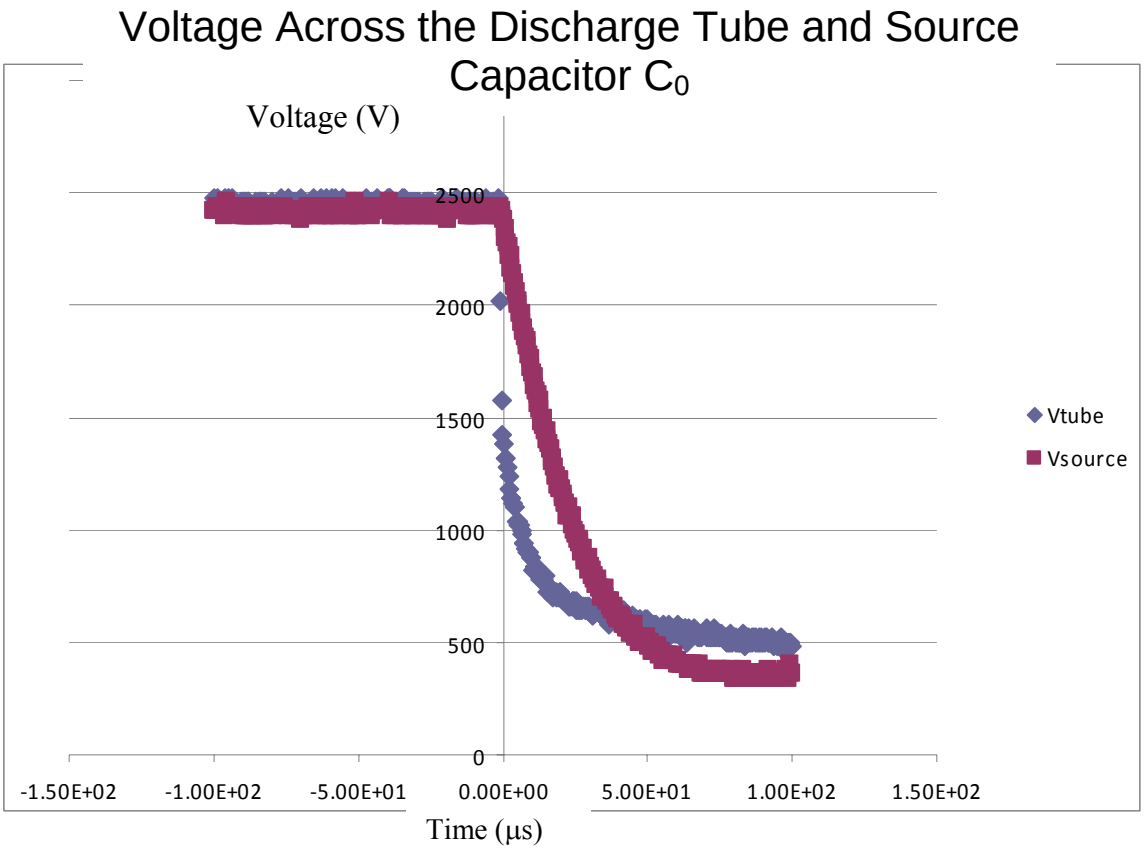
Voltage Across the Discharge Tube and Source Capacitor C_0
Voltage (V)
2500
2000
1500
1000
500
0
-1.50E+02
-1.00E+02
-5.00E+01
0.00E+00
5.00E+01
1.00E+02
1.50E+02
Time (μs)
Vtube
Vsource

(c)

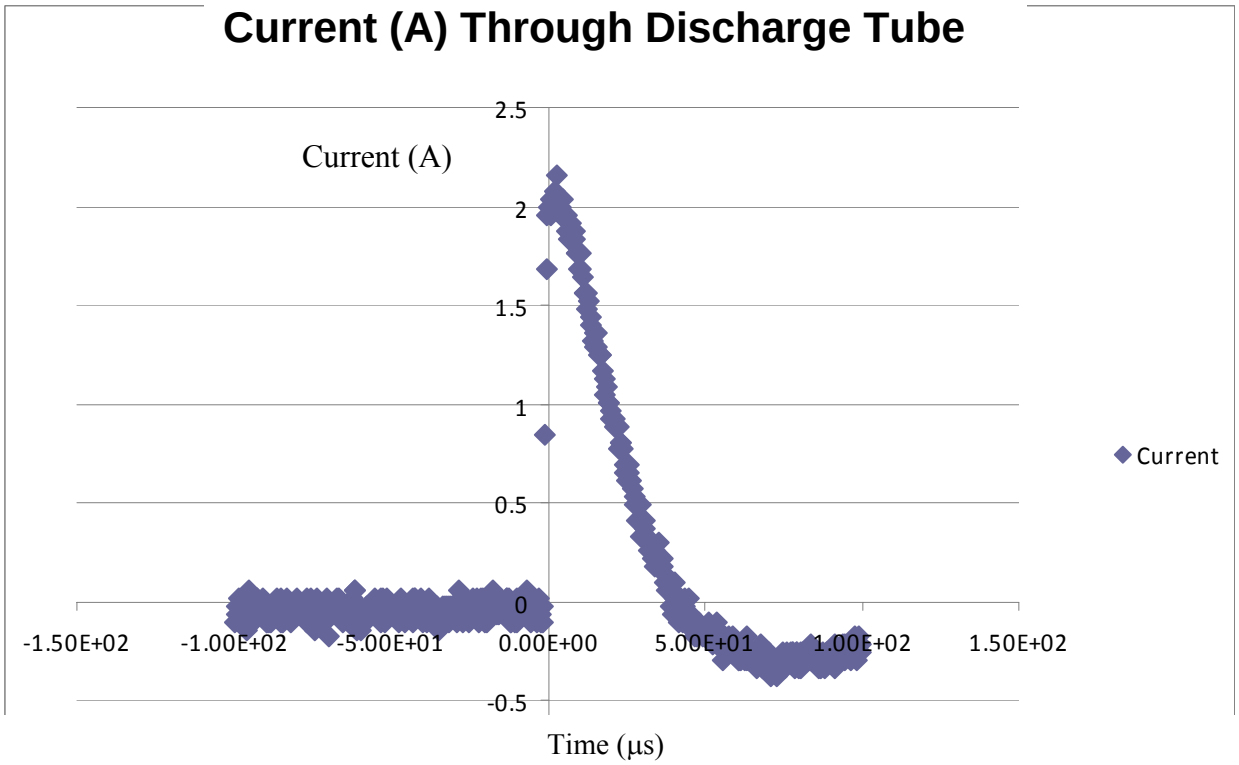
Current (A) Through Discharge Tube
Current (A)
2.5
2
1.5
1
0.5
0
-0.5
-1.50E+02
-1.00E+02
-5.00E+01
0.00E+00
5.00E+01
1.00E+02
1.50E+02
Time (μs)
Current

(d)

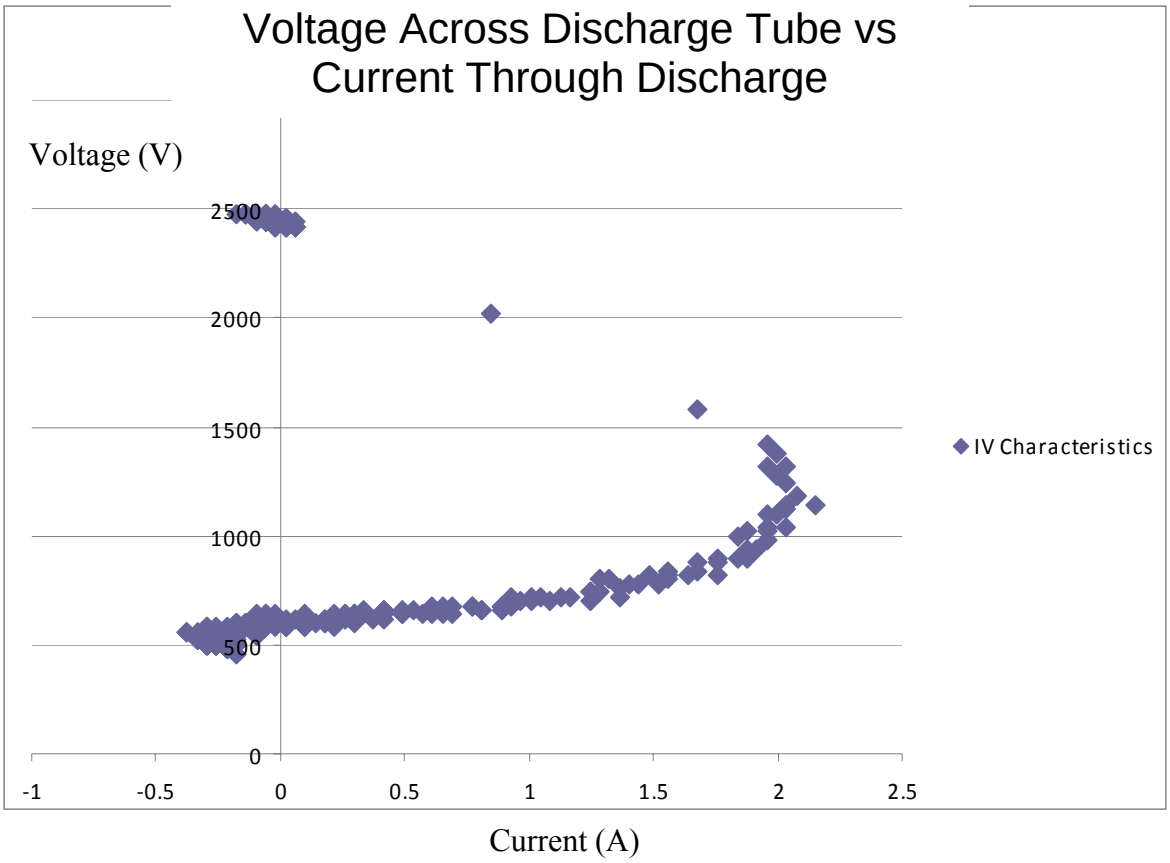

(e)

Fig. 13a-e Typical a) discharge tube set-up with b) discharge image. The c) discharge and source voltage and d) discharge current are both plotted against time. Using time as the parametric parameter, the e) discharge voltage is plotted against discharge current data. Figures (a) and (b) are not electronically altered in size from the original camera generated picture. Table 2 contains the experimental parameters coinciding with this data set. Note the overall dimension of the discharge. The discharge is not continuous over time (repetition rate of about 1 Hz) but the shape of the discharge and its discharge location appears nearly independent of time. The voltage-current characteristics clearly show the charge and discharge transition signature of the discharge.

VI. Electron Channeling in a Nearly DC-Like Discharge Tube

A simple nonlinear theory is developed to estimate the process of electron channeling for an energetic electron beam passing through a cool plasma. The motivation of the theory is to determine if the fast moving secondary electron emission particles passing through a discharge may be responsible for the pinch effect that seems to appear in experiments.

The discharge is assumed composed of three interpenetrating charged gas species: ion fluid and two electron fluids with significantly different initial states. The ion species is assumed massive enough under the time frame of the experiment such that its sluggish motion may be assumed nearly zero. A cool thermal electron fluid of nearly the same initial density of the ion fluid is assumed to have a zero initial drift velocity. Since the electron and ion fluids are cool, their thermal effects are neglected. Further, quasi-neutrality between the two fluids is imposed

initially. A cold energetic electron fluid with uniform density, denoted as the electron beam, is injected in the plasma medium. The electrons are so energetic that the divergence of the electron beam due to space charge effects in the plasma medium may be assumed small over the duration of the experiment within the overall length of the plasma gas. Although thermal effects have been neglected, it is assumed that the multiple species gas has enough thermal energy to minimize recombination on time scales of the experiment. Further, the injected electron beam is a continuous source of energetic charge over the duration of the experiment. Consequently, the radial drift velocity of the electron beam is negligible over the entire length of the plasma.

Under these and other constraints, the governing relations for the jth species are

$$\frac{\partial n_j}{\partial t} + \vec{\nabla} \cdot [n_j \vec{v}_j] = 0 \tag{21a}$$

$$m_j n_j \frac{d\vec{v}_j}{dt} = n_j q_j E_r \hat{r} \tag{21b}$$

$$\oiint_S \vec{E} \varepsilon_o \cdot d\vec{S} = \iiint_v [q_b n_b + q_i n_i + q_e n_e(\vec{r},t)] d\mathcal{V} \tag{21c}$$

where j=b, i, e representing the beam electron fluid, cool thermal ion fluid, and the cool electron fluid respectively and $\vec{E}$ is the resultant electric field in vacuum with permittivity of free space, ε_o. Here, m_j, n_j, q_j, and $\vec{v}_j$ are respectively the mass, number density, the charge, and average fluid velocity of the jth species.

It is assumed that the density is uniformly distributed with respect to radius and changes uniformly with time. Under this and other inherent assumptions not explicitly stated, the internally self-consistent relation can be obtained based on Eqs. (21a-c)

$$\frac{dn_e(t)}{dt} + \sqrt{\frac{2e^2}{\varepsilon_0 m_e}} [n_e(t) - n_i + n_b]^{1/2} n_e(t) = 0 \tag{22}$$

A number of perturbation techniques were used to solve this relation. These were then compared against the numerical simulation of Eq. (22). Analytical expressions usually allow for global interpretation of the physics within the context of the perturbation. Only one perturbation case and one exact case to the solution of Eq. (22) are presented here for brevity. This work is being prepared for publication. Full details and numerous comparisons will be presented at that time.

Case 1: $n_b = n_i$

Under the special case in which the initial energetic electron beam density equals the ion beam density, Eq. (22) simplifies to

$$\frac{dn_e}{dt} + \sqrt{\frac{2e^2}{\varepsilon_0 m_e}} n_e^{3/2} = 0 \tag{23}$$

Solving, one can show that

$$n_e(t) = \frac{n_{eo}}{\frac{1}{2}\omega_{pe}{}^2 t^2 + \sqrt{2}\omega_{pe} t + 1} \tag{24}$$

where $\omega_{pe} = \left[e^2 n_{eo} / \varepsilon_o m_e\right]^{1/2}$ is the electron plasma frequency. Initially (t=0), the electron density is the initial plasma density. As time approaches infinity, the thermal electron density approaches zero as expected. From Eq. (24), one can determine the time it takes for beam pinching to be initiated by electron channeling.

Case 2: $n_i - 0.5 n_e(t) >> n_b$

Typically, one would expect that the beam density is lower than the plasma density. Applying a unique perturbation technique, it can be shown that

$$n_e(t) = n_i - n_b + \frac{2n_{e0}\left[\sqrt{2n_b n_{e0}} - (n_i - n_b)\omega_{pe} t\right]^2}{\left[\sqrt{2n_b n_{e0}}\,\omega_{pe} t - \frac{1}{2}(n_i - n_b)\omega_{pe}^2 t^2 + 2n_{e0}\right]^2} \tag{25}$$

Initially (t=0), the density of the cool thermal charge equals the background ion density as required for quasi-neutrality. This relation is meaningful only over the time interval $0 \le t \le t_{\max 3}$. As time t becomes large, Eqs. (25) must approach zero yielding a minimum energy state. This condition is satisfied only if

$$t_{\max 3} = \frac{2\sqrt{n_b}}{A(n_i - n_b)}. \tag{26}$$

As time t approaches t_{max3}, the thermal electron density approaches the ion density minus the energetic electron beam density; $n_i - n_b$ as expected.

These two cases as well as the others not presented have shown good agreement to appropriate segments of the general relation Eq. (22) solved numerically. Currently, experimental studies are under way to determine if one can relate the stability time intervals to the formation of the discharge in the lab. Further, there are some special asymptotic density threshold conditions which dictate whether pinch formation will result. The latter condition appears experimentally promising to verify.

VII. AFOSR/UNLV High School Teacher Summer Laboratory Research Experience - Equilibrium Plasma Pinch in a Discharge Tube [2008, 2009]

In the summer of 2009, we were unable to find a sponsor to supplement the AFOSR/UNLV research experience funds; therefore, only one high school teacher was sponsored. In the summer of 2008, we funded two high school teachers. In short, high school

teachers would shadow students and staff in the Energy Materials Interaction Technology Initiative of Nevada (EMITION) Center at UNLV for 20 hours a week over an eight week period. They would be tasked a research effort in support of this grant. The effort leads to an experiment with design, data acquisition, analysis, and theory. At the end of the research effort/experience culminating with a report, the equipment and experiment are permanently transferred to the high school that the teacher resides at for incorporation into the high school teacher's science/mathematics curriculum for high school students. During the course of the summer laboratory experience, the teacher performs a valuable function in working on a problem of national interest, learn basic science of use to his/her own career, and pass this valuable experience onto his/her students in high school science, technology, engineering and/or math (STEM) classes. The overall goal is to motivate young minds into STEM fields. It is anticipated that the high school teacher will talk up his/her experience to his/her class while performing various demonstrations and hands on experiments associated with the experience. The high school teacher is encouraged to invite his/her class to the EMITION Center at UNLV for tours and interactions. Consequently, one component of the report contains high school lesson plans incorporating some aspect of the experiment into high school courses taught by the teacher. Indirectly, AFOSR through the high school teacher mentor is motivating and stimulating the young minds of US citizens to enter the science, technology, engineering, and mathematics fields. Already, the need for such minds is affecting the fabric of our nation to lead the world in technology especially important to DOD. [Upon request, the reports are available. Typically, the reports are over 50 pages in length.]

During the summer 2008, two teachers designed and built a simple DC discharge tube to investigate some aspects of the physics pertinent to that in the take-off region of a non-equilibrium plasma pinch (NEPP). The uniform generation of the plasma sheath in this region dictates the nature of the pinch. In the process of that study, a noticeable unexpected pinch effect was observed which appears relevant to pinch physics. In the summer of 2009 with the aid of the EMITION staff, the teacher sponsored experimentally re-examine the discharge phenomenon that exhibited the properties of the equilibrium pinch. Figures 14a,b display the DC discharge with ancillary equipment and provides a close-up view of the simple discharge tube.

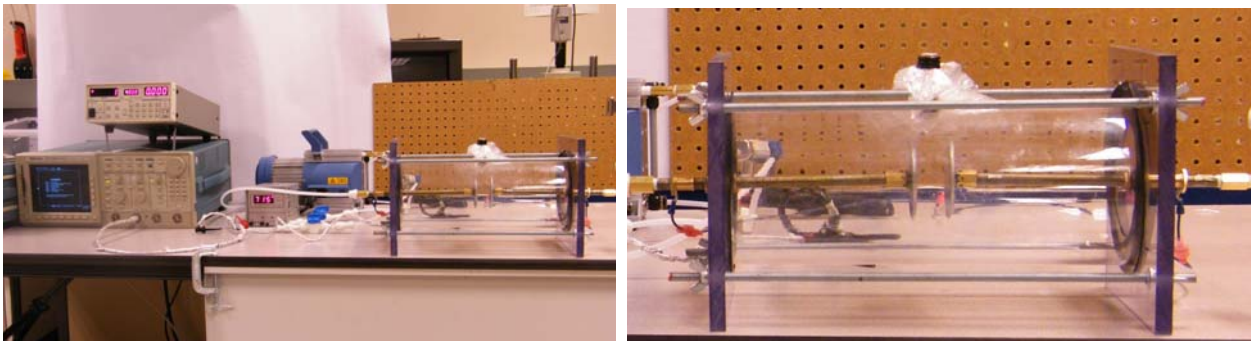

Fig. 14a,b The a) DC discharge tube setup with a b) close-up view of the discharge tube.

A number of observations were uncovered. First, originally the vacuum pressures were measured with a thermal couple gauge. Thermal couple gauges have a working pressure range between about 1 mTorr to about 10 Torr. Pressures beyond 10 Torr are not accurately measured. Since some of the experimental pressures exceeded the 10 Torr range, the pressure gauge inaccurately measured the discharge tube's pressure at the higher pressures. The thermal couple gauge was replaced by a convectron gauge with a pressure range typically between 1 mTorr to

1000 Torr. (For reference, one atmospheric pressure is 760 Torr; 1Torr is 133.33 Pa.) When the experiments were performed in 2009, the same discharge properties were observed but at pressures that were considerably lower. Second, how the discharge formed is partially dependent on the initiation of the discharge. Three scenarios were examined: discharge initiation as the pressure fell, as the pressure was raised, and at a nearly constant pressure. Limiting the current at a constant voltage also played a role in the formation and strength of the discharge. Figure 15 provides the discharge geometry at four different pressures with the same source conditions. Notice the difference in the plasma radius as determined by the visible radiation due to recombination or relaxation. Third, to demonstrate that indeed we have a pinch condition, the pressure was maintained constant and the current draw was controlled by changing the current threshold ether to limit the current draw or allow for more current draw at the pinch. Although not displayed here, using MATLAB tools based on the optical intensity of the discharge, the diameter of the pinch decreased as the current was allowed to increase. This is the sign of a pinch. Fourth, cleanliness of the electrode surface plays a significant role on the type of discharge generated. The rougher the electrode surface is, the greater the probability that the discharge is an arc like discharge as compared to a glow like discharge. Arc-like discharges are sporadic and tend to further degrade the electrode surface. Glow-like discharges minimize electrode degradation and appear more controllable exhibiting a consistent discharge pattern over time.

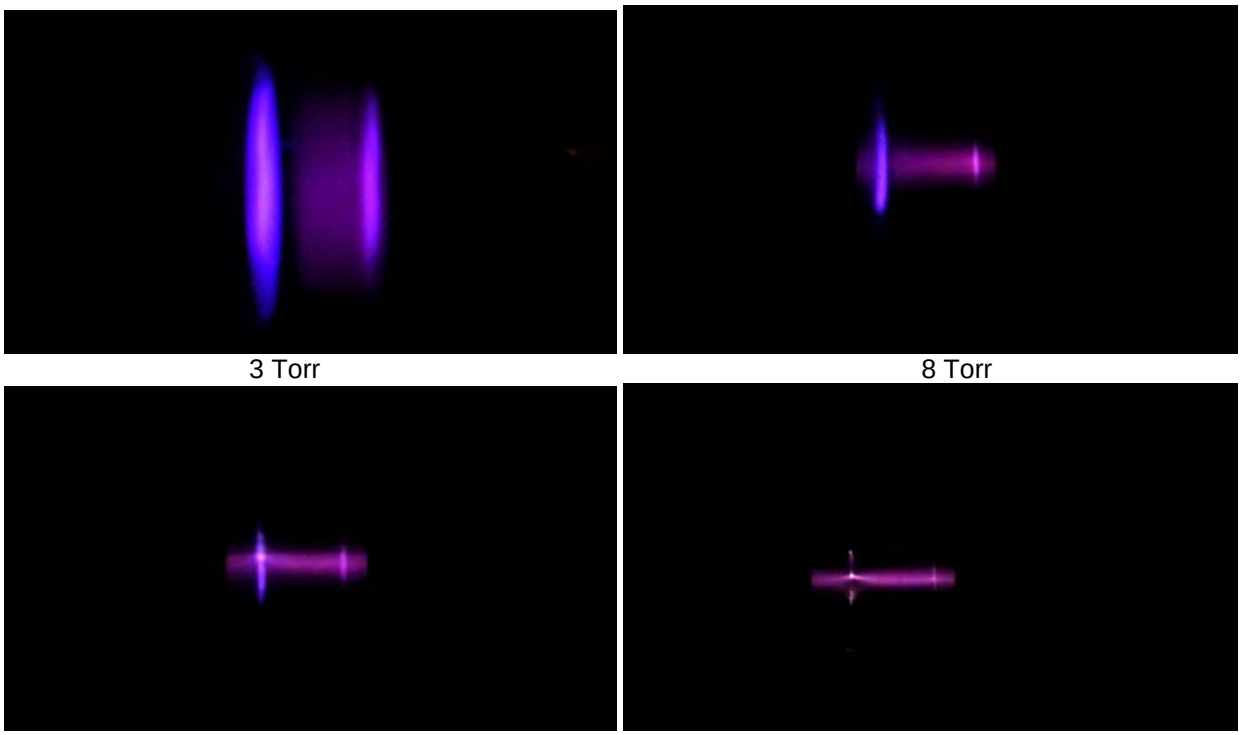

Fig. 15 Plasma discharge at various pressures near breakdown for the same source conditions.

VIII. Conclusion

Over the past three years, great strides have been made in building the analytical and experimental infrastructure to study pinch physics for plasma cathodes in high power microwave (HPM) devices. In the process, a patent is pending on a beam management device and a calibration scheme with theory was developed for the EM dots to be used in pinch experiments. The NEPP was designed, built, and tested in the past two years and a magnetron shell with emission element has been coupled to the NEPP. Two high school teachers benefited from the research which in turn resulted in an unexpected research effort leading to the study of the non-equilibrium pinch. This research endeavor was picked up by an MS candidate in the past year. A recently developed theoretical study is currently being verified by experiment. A number of US students benefited from the research in various capacities. Although we have not completely addressed the hypotheses underpinning the original proposal, there is some indication that secondary electron emission may play a role in both equilibrium and non-equilibrium pinch physics. We currently have the infrastructure to further pursue this study. New research has spawned from this study of potential benefit to AFOSR and DOD.

Appendix A
PPC 2009 Washington, DC

ELECTROMAGNETIC DOT SENSOR – CALIBRATION*

A. Al Agry, R. A. Schill, Jr., S. Garner, S. Andersen, and K. Buchanan
Department of Electrical and Computer Engineering
University of Nevada Las Vegas
4505 Maryland Parkway
Las Vegas, NV 89154-4026 USA

Abstract

The recently patented UNLV Electromagnetic (EM) dot sensor measures the rate of change of the electric flux density and the magnetic flux density at the same point in space simultaneously over time. This single device performs the function of two to four sensors distributed in space. The calibration setup of the EM-dot is presented ultimately leading to a pair of calibration factors.

I. INTRODUCTION

The measurement of transient and AC, narrow-band and broad-band, electromagnetic (EM) fields and related parameters finds application in various kinds of electromagnetic environments. One electromagnetic application is the pulsed power system (electromagnetic pulse (EMP), lightning, charged particle beam), where fast, large amplitude pulses are encountered. In the pulsed power application, one has to measure transient electromagnetic fields and related quantities, therefore, accurate broadband sensors with simple transfer functions are needed.

Diagnostic detectors extend from thermal probes, to polarization probes, to small integrating probes. The resistive sensor is an electromagnetic device whose performance is based on the electron heating effect in semiconductors. When a strong electric field pulse is applied to a semiconductor, a new steady state condition is achieved with mean electron energy much greater than the equilibrium energy [1-2]. Electro-optic and magneto-optic sensors can also be utilized to measure pulse parameters. A typical electric field sensor uses the Kerr effect, which is a polarization sensitive optical effect. The magnetic field sensor uses the Faraday effect that appears as a rotation of the polarization plane of a light wave traversing a medium. Alternative technique for measuring the electric field uses the Franz-Keldysh effect, which refers to the electric field sensitivity of the optical absorption coefficient in semiconductors. Since these sensors directly measure the signal of interest rather than the time derivative, they become more attractive for long-pulse applications in the microsecond regime with slow rise time [3-5]. Small integrating probes commonly known as B-dot and D-dot probes have existed for decades [6-9]. These probes are quasi-electromagnetic sensors in the sense that they respectively transform the electromotive force (inductively coupled magnetic field) and the magnetomotive force (capacitively coupled electric field) into a voltage and a current allowing for the measurement of the rate of change of the magnetic flux density [B-dot] and the electric flux density [D-dot]. In general, these electromagnetic sensors are based on electric and magnetic dipole moments, being the leading terms in a multipole expansion [10].

The passive, wideband, symmetric, time integrating, patented (now US Patent Number: 7,482,814 [1/27/2009] and subject to International Patent Application No.: PCT/US2006/033453 based on U.S. Patent Application No.: 11/213,628), UNLV, EM-dot sensor measures the change in the electric field and the change in the magnetic field simultaneously over time at one point in space [11]. The time-integrated device is sensitive enough to monitor electric field to magnetic field transitions and vise versa as characteristic changes occur. Typically, one device does the job of two or more devices. Monitoring transitions in the fields indirectly monitors transitions in the voltages and currents in a circuit. In [11], a theoretical structure and model with calibration procedure and results were presented. In this paper, the calibration setup is pictured and elaborated on.

This paper is formatted in the following manner. Section II provides the calibration setup. Calibration results are presented in Sect. III. Conclusions are stated in Sect. IV.

* This work was supported by the AFOSR under contract numbers FA9550-06-1-0451 and FA9550-08-1-0045.

II. CALIBRATION SETUP

Figure 1 displays a typical EM-dot sensor.

Figure 1. Typical size of the dot illustrated

The calibration studies were conducted with a 3148 Bournlea Pulse Generator with a measured rise (fall) time of 6 ns, and a pulse width of 24 ns. The 50 Ω input impedance pulser supplies a 1 kV peak Gaussian like pulse to a 551.18 cm long Z_0=50 Ω coaxial cable with a velocity of propagation of ~70% of the speed of light to:

- a 50 Ω ½ W resistor in series with 66.12 nH solenoid (B-dot calibration test stand);
- a 50 Ω ½ W resistor in parallel with a small geometry 2.3 pF parallel plate capacitor (D-dot calibration test stand).

Lead lines connecting the loads above to the line are kept as small as possible and all lumped components are kept as close together as possible.

A Stanford Research Inc. Four Channel Digital Delay/Pulse Generator, Model DG535 was used to control the Bournlea pulser in single shot mode. All studies performed were conducted in single shot mode. The output high voltage of the Bournlea pulse generator is sampled internally at the output high voltage port through a 60 dB attenuation pad. A transmission line of length nearly equal to the dot's connecting lines, guides the output monitor signal to a 6 GHz bandwidth, real time, TDS 6604 Tektronix Oscilloscope. The internal 60 dB attenuation pad was not tested for accuracy.

Each transmission line cable connecting the EM-dot to the real time oscilloscope was placed in an adequately grounded copper tube. The copper tube was grounded both on the oscilloscope and on the calibration test stand sides. The output monitor coaxial line was positioned far from the experimental test stands so to minimize signal coupling on the line since it was not specially shielded like the dot lines. The output monitor signal is used for comparison.

When a pulsed high voltage signal is applied to a resistor, the resistance of the resistor my exhibit nonlinear effects even though the resistor is operating at temperatures within specification. The effect of 50 Ω, 0.5 W carbon resistor at the end of a 5.51 m transmission line is examined and compared to standard off-the-shelf single port 50 Ω loads when a 1 kV, 24 ns pulsed voltage is applied to the transmission line. Fig. 2a displays a 5.51 m line with SMA connectors with one side connected to the Bournlea pulser and the other terminated in a manufactured single port 50 Ω load matched load. The signal signature shown in Fig. 2a indicates minimal reflection as a consequence of this load. In comparison, two standard 100 Ω 0.25 W resistors in parallel yielding an equivalent 50 Ω 0.5 W resistor is examined under the same conditions as shown in Fig. 2b. As observed in Fig. 2b, there is a significant reflected signal as a consequence of the thin film resistors as compared to the case of the single port termination shown in Fig. 2a. Consequently, it is anticipated that some reflection will result in the calibration studies as a consequence of the resistive loads being employed for matching purposes.

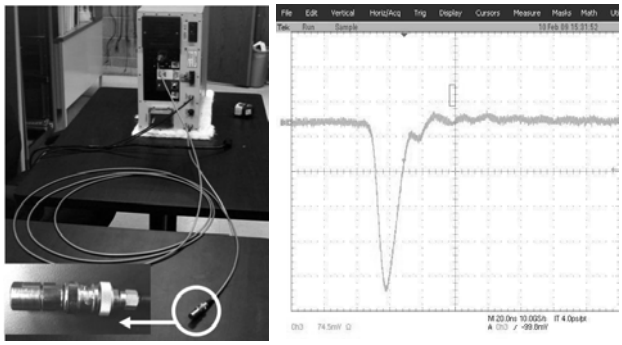

2a

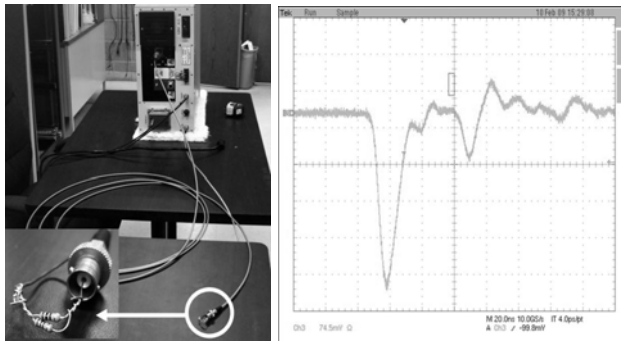

2b

Figure 2a,b. A 5.51 m coaxial cable transmission line connected to the high voltage output terminal of the Bournlea pulser is terminated into (a) conventional 50 Ω termination, (b) a lumped 50 Ω thin film ½ W resistor (or equivalently a parallel combination of two ¼ W, 100 Ω resistors). As shown in the displayed signal signature (b) the equivalent thin film resistor does not terminate the line in a matched load. The Bournlea source is set for an output peak voltage of 1 kV.

Once the dot signals have been generated, they are appropriately processed with a math channel internally in the oscilloscope and/or externally processed with data acquisition software. In some cases, the externally

processed integrated signal will exhibit a linear drift resulting in the pulse signature riding on a linear ramp signal signature. A linear voltage versus time line is fitted to the initial noise of the data where the integrated signal is suppose to be zero. This is then subtracted from the time integrated processed data in a point-by-point manner over the entire duration of the signal. The data processed by the math channel internal to the scope does not display a significant linear shift in time due possibly to the resolution of the display. Using external data acquisition software, the integrated sensor signals were then shifted in time so that the signal signatures overlapped with the Bournlea Output Monitor signal. Finally, the amplitude is adjusted until a single calibration factor provides the best fit with the Bournlea Output Monitor signal. Based on theory, certain features of the signal should agree. These features are taken into consideration when comparing signals in the curve comparison process.

A. *B-dot Mode Calibration Setup*

The B-dot calibration test stand composed of a low inductance air solenoid with cross sectional area similar to that of the EM-dot under test in series with a $R_m = 50\Omega$ matching resistor provided superior magnetic field calibration properties yielding textbook results. Because the EM-dot in B-dot mode is orientation sensitive, the dot is placed in a central location between the solenoid ends with the solenoid and loop nearly sharing the same axis. Further, due to the geometric symmetry of the dot, twisting the loop area 180 degrees, excluding an overall sign change, should make no difference in the response of the dot. This result was observed. Moreover, the solenoid due to its material properties acts as a partial shield to externally generated noise. This is important since all calibration studies are performed in a laboratory environment without noise control.

As the solenoid coil diameter and/or the number of turns increases, the inductance increases. The increase in inductance results in pulse broadening as a consequence of the increase in response time (time constant) of the inductor. If the number of turns is too small, the assumed uniformity of the axially directed fields internal to the solenoid is compromised. After a number of test cases were examined, a six-turn solenoid proved optimal for calibration purposes. The six-turn solenoid (two sets of three turns) was composed from typical doorbell stock wire with a wire diameter of 0.65 mm and a wire with insulation diameter of 1.12 mm. The inside and outside diameter of the solenoid are respectively 2.93 mm and 5.16 mm. Consequently, the average diameter of the solenoid is 4.04 mm and the distance of separation between turns is 1.12 mm. The total length of the six-turn coil with a 2.76 mm gap between turns 3 and 4 for the EM-dot sensor loop is 11.33 mm. Because of the large gap in the solenoid, the solenoid is treated as two inductors connected in series. Consequently, two series N=3 turn $l = 4.29$ mm long, 4.04 mm diameter (cross sectional area $A = 1.28\times10^{-5}$ m^2), air filled ($\mu_0 = 4\pi\times10^{-7}$ F/m) solenoids have an estimated inductance of 0.03 μH each or a total estimated inductance of 67 nH (estimated total inductance $L_{est} = 2\left(\mu_0 AN^2\right)/l \approx 0.067\mu H$). Using a modified Maxwell-Wein bridge as shown in Fig. 3, the measured inductance L is 66.12 nH.

The bandwidth of the test stand to minimize pulse broadening and maximize amplitude tracking is [11]:

$$f \le 0.35\frac{\left(R_m + Z_0\right)}{10L} \tag{1}$$

Numerically, the bandwidth of the test stand is 53 MHz for this calibration setup. For a measured rise time of approximately 6 ns, the bandwidth of the Bournlea pulse is about 58 MHz [11]. The bandwidth of the Bournlea pulse exceeds the bandwidth of the connecting load circuit by about a factor of 1.1 implying that the calibration circuit amplitude differences and pulse broadening should be expected but this is not due to the limitations of the EM-dot. It is due to the loading effect of the test stand itself.

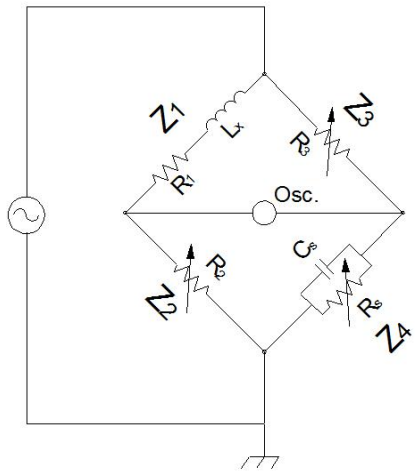

Figure 3. Sketch of the modified Maxwell-Wein bridge used to determine the inductance of the solenoid coil used in the B-dot calibration test stand.

Figure 4 illustrates the calibration setup in an open laboratory. To minimize the interference with the surrounding environment, the coaxial cables connecting the EM-dot to the oscilloscope have been shielded with a rigid copper tube. Each line could have their own rigid tube or share a rigid tube. The use of triaxial cables would have performed the same function. The open ends of the copper tube are covered with aluminum foil that extends to and covers the oscilloscope ground connector on the scope side and the dot assembly up to

but not including the sensors loop wire on the sensor side. We have noticed that low-level noise can be induced in the shielding of the oscilloscope. To reduce the noise level, the oscilloscope was positioned as far as possible from the pulser. In the calibration studies, the distance between the oscilloscope and pulse generator was about 551.18 cm.

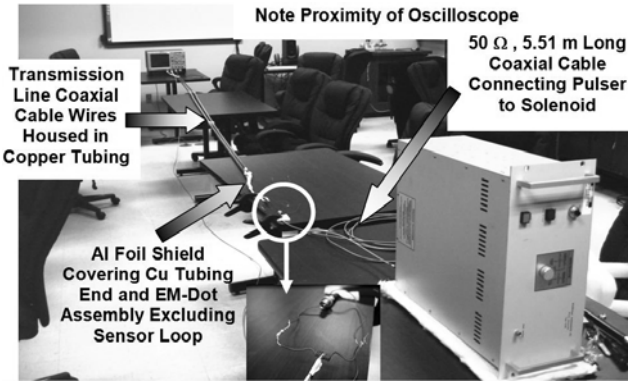

Figure 4. The experimental setup for calibrating the EM-dot in B-dot mode. Note the proximity of the oscilloscope, extra copper tubing and aluminum foil shielding. The B-dot calibration test stand is composed of a 50 Ω 0.5 W matching resistor in series with two 3 turn, 4.29 mm long, 4.04 mm average diameter solenoids having a total inductance of 66.12 nH.

B. ***D-dot Mode Calibration Setup***

The D-dot calibration test stand composed of a low capacitance, geometrically small, parallel plate capacitor in parallel with a $R_m = 50\Omega$ matching resistor was chosen as the means for calibrating the EM-dot in D-dot mode. The small plate geometry allows the capacitor to be treated as a lumped capacitor. A sketch of the experimental setup is provided in Fig. 5.

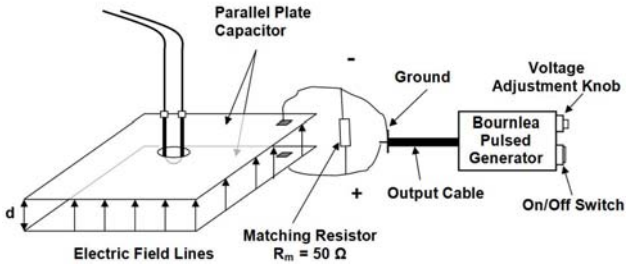

Figure 5. Experimental setup for calibrating the EM-dot in D-dot mode. The sensor end of the EM-dot assembly extends just beneath the upper plate. The capacitor is connected to the pulse generator output.

With plates isolated far from external metal objects (at least ten times the distance of separation between the plates), the field concentration is contain mainly between the plates. The sensor is inserted normal through a hole in the center of the grounded capacitor plate such that the sensor end of the dot is just beneath the surface of the grounded plate in between the plates. The grounded plate is attached to the semi-rigid coaxial waveguides and other external tri-shielding material of the dot assembly. The 6.5 cm × 6 cm plates with a 1.5 cm distance of plate separation allow for uniformity of the signal near the dot and minimize fringing and radiation effects with the shielded and unshielded connecting cables external to the capacitor. The capacitance of the air dielectric parallel plate capacitor is C = 2.3 pF. The Bournlea pulsed generator (Fig. 5) was operated at the 1 kV peak level. The bandwidth of the test stand to minimize pulse broadening and maximize amplitude tracking is [11]:

$$f \le 0.35 \frac{1}{10C\left(R_m Z_0 / \left(R_m + Z_0\right)\right)} \qquad (2)$$

Numerically, the bandwidth of the test stand is about 609 MHz. The bandwidth of the Bournlea pulser (58 MHz) is well within the bandwidth of the RC test stand.

Figure 6 illustrates the calibration setup in an open laboratory. Similar to Fig. 4, the coaxial cables connecting the EM-dot to the oscilloscope have been shielded with a rigid copper tube. The open ends of the copper tube are covered with aluminum foil that extends to and covers the oscilloscope ground connector on the scope side and the dot assembly up to but not including the sensors loop wire on the sensor side. To reduce the noise level, the oscilloscope was positioned as far as possible from the pulser. In the calibration studies, the distance between the oscilloscope and pulse generator was about 551.18 cm.

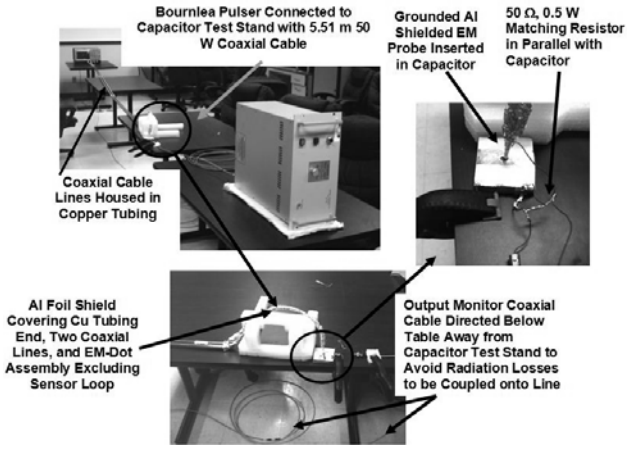

Figure 6. The experimental setup for calibrating the EM-dot in D-dot mode. Note the proximity of the oscilloscope, extra copper tubing and aluminum foil shielding. The D-dot calibration test stand is composed of a 6.5 cm × 6 cm × 1.5 cm, C=2.3 pF capacitor in parallel with a 50 Ω 0.5 W resistor. The test stand is connected to a Bournlea pulse generator with a 5.51 m,

$Z_0 = 50\Omega$ coaxial cable transmission line. The EM-dot is inserted in the grounded plate of the capacitor. The aluminum foil covering the EM-dot up to but excluding the sensor loop is electrically connected to the ground plate of the capacitor.

III. CALIBRATION RESULTS

The oscilloscope measured output monitor voltage of the pulse generator is compared with the time-integrated signal from the EM-dot in B-dot mode as illustrated in Figs. 7, and D-dot mode as illustrated in Fig. 8. As suggested by the results from Eqs. (1) and (2), excellent agreement in pulse tracking is observed visually up to the base of the reference signal. Quantitatively, the relative percent error for the fall time, pulse width (FWHM), and rise time relative to the output monitor signal for the B-dot mode are: 8%, 12%, 76.2% respectively, while for the D-dot mode: 24.2%, 3.2%, 17.1% respectively. Further, as predicted in the theory leading to Eqs. (1) and (2) when the line is *mismatched* [11], some bandwidth broadening may result and tracking will become less accurate. Just beyond the base of the pulse in Fig. 7, loading effects of the inductor with matched resistor are apparent.

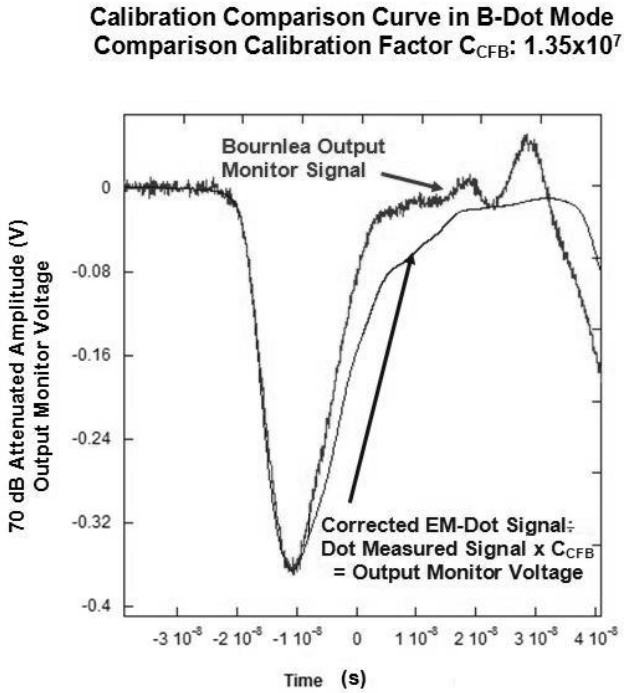

Figure 7. Fitted curves for EM-dot to the Bournlea output monitor signal. The sensor signal measuring the magnetic field is linked directly to the current. The signal signature of the Bournlea pulser as measured at the oscilloscope is attenuated with attenuation pads totally 70 dB. The time-integrated signal as measured in the low inductance solenoid in series with a matching resistor multiplied by the comparison calibration factor C_{CFB} is also displayed visually showing a good fit to the Bournlea signal. The EM-dot is inserted in the center of the six-turn solenoid. The pulser output voltage is set for 1 kV.

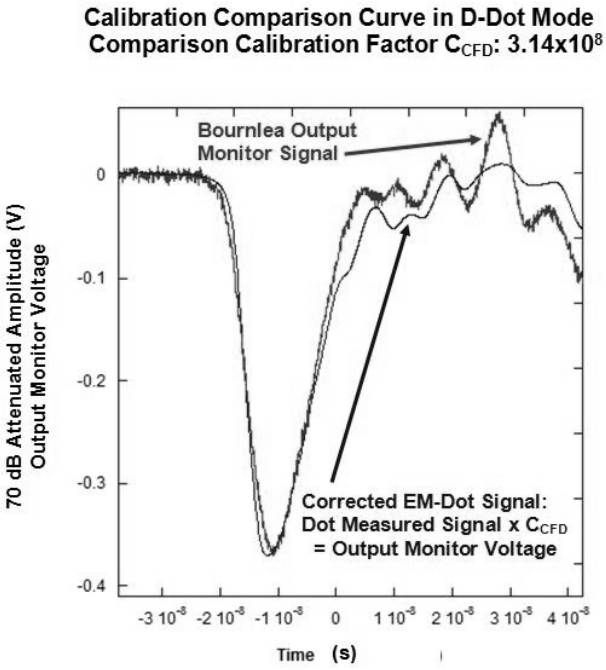

Figure 8. Fitted curves for EM-dot the Bournlea output monitor signal. The sensor signal measuring the electric field is linked directly to the output voltage of the Bournlea pulser. The time-integrated signal as measured in the low capacitance parallel plate capacitor (2.3 pF) in shunt with a matching resistor multiplied by the comparison calibration factor C_{CFD} is also displayed visually showing a good fit to the Bournlea signal. The sensor tip of the EM-dot is inserted in between the capacitor plates just beyond the surface of the ground plate at the center of the ground plate. Some of the loop area may be exposed in between the plates. The dimension of the air filled 2.3 pF capacitor is: 6.5 cm × 6 cm x 1.5 cm. The pulser output voltage is set for 1 kV.

IV. CONCLUSIONS

A novel EM-dot has been calibrated for measuring both the electric and magnetic fields. The calibration results of the EM-dot show good agreement with the reference output signal of the pulse generator as predicted by theory.

REFERENCES

[1] M. Dagys, Z. Kancleris, R. Simni_kis, E. Schamiloglu, F. J. Agee, A. Go_tauto "Application of Resistive Sensors for Short High-Power Microwave Pulse Measurement", 12th IEEE Pulsed Power Conference, 1999, pp 829-832 vol. 2.

[2] Z. Kancleris, M. Dagys, R. Simniskis, E. Schamiloglu, F. J. Agee "Recent Advances in HPM Pulse Measurement Using Resistive Sensors", 14th IEEE International Pulsed Power Conference, 2003, pp 189-192 vol. 1.

[3] M. A. Brubaker, C. P. Yakymyshyn, A. J. Iverson and I. E. VandeVeegaete "A Prototype Optical Voltage Sensors for Accelerator Diagnostic Applications", 12th IEEE International Pulsed Power Conference, 1999, pp 619-622 vol. 2.

[4] B. T. Neyer, J. Chang, G. J. Lockwood, and L. E. Ruggles "Calibrated Farady Current and Magnetic Field Sensor", 5th IEEE International Pulsed Power Conference, 1985, pp 389-392.

[5] Lynn R. Veeser, Robert S. Caird, Bruce L. Freeman, Don R. Kania, Peter J. Kruse, Robert J. Trainor, and Eugene L. Zimmermann "Single Mode Fiber Optic Sensor for High Currents", IEEE power electronics specialists conference, 1983.

[6] C. E. Baum "Sensors For Measurement of Intense Electromagnetic Pulses", 3rd IEEE International Pulsed Power Conference, 1981, pp 180-185.

[7] W. A. Stygar, R. B. Spielman, H. C. Ives, W. B. S. Moore, J. F. Seamen, and A. W. Sharpe "D-Dot And B-Dot Monitors for Z-Vacuum-Section Power-Flow Measurements", 11th IEEE International Pulsed Power Conference, 1997, pp 1258-1263 vol. 2.

[8] Carl E. Baum, Edward L. Breen, Joseph C. Giles, John O'Neill and Grady D. Sower "Sensors for Electromagnetic Pulse Measurements Both Inside and Away from Nuclear Source Regions", IEEE Transaction on Antennas and Propagation, 1978, vol. 26, issue 1.

[9] Gary Sower "I-Dot for Pulsed Power Monitors", 3th IEEE International Pulsed Power Conference, 1981, pp 189-192.

[10] Carl E. Baum "From the Electromagnetic Pulse to High-Power Electromagnetics", Proceeding of the IEEE, 1992, vol. 80, issue 6.

[11] A. Al Agry, R.A. Schill, Jr., and S. Garner, submitted to the Review of Scientific Instruments.